An epigenetic switch regulates the ontogeny of AXL-positive/EGFR-TKI resistant cells by modulating miR-335 expression.

Debjani Pal[1,2†], Polona Safaric Tepes[1,3†], Trine Lindsted[1], Ingrid Ibarra[1], Amaja Lujambio[5], Vilma Jimenez Sabinina[1], Serif Senturk[1], Madison Miller[1], Navya Korimerla[1,4], Jiahao Huang[1], Larry Glassman[6], Paul Lee[6], David Zeltsman[6], Kevin Hyman[6], Michael Esposito[6], Gregory J. Hannon[1,7], Raffaella Sordella[1,8,*]

1. Cold Spring Harbor Laboratory, 1 Bungtown Road, Cold Spring Harbor, NY 11724

2. Graduate Program in Molecular and Cellular Biology, Stony Brook University, Stony Brook, NY 11794

3. Faculty of Pharmacy University of Ljubljana, Askerceva cesta 7,1000 Ljubljana, Slovenia

4. Graduate Program in Biomedical Engineering, Stony Brook University, Stony Brook, NY 11794

5. Icahn School of Medicine at Mount Sinai, Hess Center for Science and Medicine, New York, NY 10029

6. Northwell Health Long Island, Jewish Medical Center, 270-05, 76th Avenue, Queens, NY 11040

7. Cancer Research UK – Cambridge Institute, University of Cambridge, Cambridge, UK

8. Watson School of Biological Sciences, Cold Spring Harbor Laboratory, Cold Spring Harbor, NY 11724

**Corresponding Author*

†*These authors contributed equally to this work.*

ABSTRACT

Lung cancer remains the leading cause of cancer-related mortality worldwide, despite current advancements in research and therapeutics. Many patients diagnosed with lung cancer will develop resistance to chemotherapeutic agents. In the context of non-small cell lung cancers (NSCLC) harboring EGFR oncogenic mutations, augmented levels of AXL and GAS6 have been found to drive Erlotinib resistance in certain tumors with mesenchymal-like features. By studying the ontogeny of AXL-positive cells, we have identified a novel non-genetic mechanism of drug resistance based on cell-state transition. We demonstrate that AXL-positive cells are already present as a sub-population of cancer cells in Erlotinib-naïve tumors and tumor-derived cell lines, and that the expression of AXL is regulated through a stochastic mechanism centered on the epigenetic regulation of miR-335. The existence of a cell-intrinsic program through which AXL-positive/Erlotinib-resistant cells emerge infers the need of treating tumors harboring EGFR-oncogenic mutations upfront with combinatorial treatments targeting both AXL-negative and AXL-positive cancer cells.

INTRODUCTION

Each year, more than a million patients worldwide are diagnosed with non–small cell lung cancer (NSCLC) (Brose, Volpe et al. 2002, Samuels, Wang et al. 2004, Stephens, Hunter et al. 2004, Haber, Bell et al. 2005, Bean, Brennan et al. 2007, Pillai and Ramalingam 2012). In 2014, the discovery that EGFR-oncogenic mutations were present in 15-30% of NSCLC patients and that the vast majority of patients harboring such mutations are particularly sensitive to treatment with EGFR inhibitors (TKi) such as Erlotinib and Gefitinib was a critical breakthrough.(Lynch, Bell et al. 2004, Paez, Janne et al. 2004). The identification of these actionable EGFR-oncogenic mutations revolutionized the management of NSCLC tumors from a predominantly clinic-pathologic to a genotype-directed classification and therapeutic approach. Yet, the success of this biomarker-based targeted therapy has been hampered by the occurrence of drug resistance. In fact, within a year of treatment with EGFR TKIs, almost all patients experience relapse (Bell, Gore et al. 2005).

The past 10 years have seen tremendous progress in our understanding of the multiple mechanisms that lead to acquired resistance against TKIs. Using both experimental systems and patient samples, secondary/gatekeeper mutations in *EGFR* (T790M), c-Met amplifications, *PI3K* mutations, and the acquisition of mesenchymal and small-cell lung cancer features have been identified and validated as molecular determinants of EGFR TKi resistance (Bell, Gore et al. 2005, Engelman, Mukohara et al. 2006, Shaw, Yeap et al. 2009, Yao, Fenoglio et al. 2010, Shaw and Engelman 2016). More recently, the expression of AXL has also been reported as an additional mechanism of acquired resistance in EGFR TKi resistant tumors with mesenchymal- like features (Zhang, Lee et al. 2012, Byers, Diao et al. 2013, Walter, Sjin et al. 2013, Elkabets, Pazarentzos et al. 2015).

AXL is a member of the TAM (Tyro-AXL-Mer) receptor tyrosine kinase family. These receptors regulate a variety of cellular responses including cell survival, proliferation, motility, as well as differentiation (Zhang, Knyazev et al. 2008, Ghosh, Secreto et al. 2011, Ben-Batalla, Schultze et al. 2013). AXL is expressed in many embryonic tissues and participates in mesenchymal and neuronal development. In adult tissue its expression is usually restricted to smooth muscle cells but it has been observed to be overexpressed in several human tumors of different tissue origins. (Zhang, Knyazev et al. 2008, Ghosh, Secreto et al. 2011, Ben-Batalla, Schultze et al. 2013).

AXL possesses an extracellular domain with two N-terminal immunoglobulin (Ig)-like domains and two fibronectin type III (FNIII) repeats that bind to the growth-arrest-specific 6 (GAS6) ligand

(O'Bryan, Frye et al. 1991, Mark, Chen et al. 1996, Nagata, Ohashi et al. 1996). The binding of AXL to GAS6 --upon its paracrine or autocrine secretion-- enables the trans-auto-phosphorylation of AXL's intracellular tyrosine kinase domain and, consequently, the activation of multiple down-stream signaling cascades (Braunger, Schleithoff et al. 1997, Prasad, Rothlin et al. 2006).

In the context of NSCLC, higher levels of AXL and GAS6 have been observed in tumors that developed resistance to Erlotinib (Zhang, Lee et al. 2012, Byers, Diao et al. 2013). In these tumors, targeting AXL by either chemical or genetic inhibition restored Erlotinib sensitivity. Alternatively, forced expression of an active AXL kinase in Erlotinib-sensitive tumor cells was sufficient to induce Erlotinib resistance (Zhang, Lee et al. 2012).

Despite these documented findings, the molecular mechanisms leading to the ontogeny of AXL-positive cells remains poorly understood. Unlike other receptor tyrosine kinases, no mutations or amplifications of the AXL locus have been described in AXL-positive/Erlotinib-resistant cells (Wu, Liu et al. 2014).

Here, we demonstrate that AXL-positive cells are already present in Erlotinib-naïve tumors and that they are generated via an epigenetic/stochastic mechanism. Consistent with this model, we found that the transition between AXL-positive and AXL-negative cells is highly plastic.

This mechanism conceptually differs from previously described models of acquired or adaptive resistance based on the acquisition of secondary mutations, or drug-driven rewiring of signaling networks. In fact, the generation of AXL-positive cells is neither generated via genetic mutations, nor dependent on the micro-environment or drug treatment (Bell, Gore et al. 2005, Engelman, Mukohara et al. 2006, Shaw, Yeap et al. 2009, Yao, Fenoglio et al. 2010, Shaw and Engelman 2016). Also different from quiescent $AKT1^{low}$ cancer cells described by the Ramaswamy group, AXL-positive cells are actively dividing (Kabraji, Sole et al. 2017).

At the molecular level, we showed that the generation of AXL-positive cells is centered on the methylation of a specific CpG island present in the promoter of *MEST*, a gene that contains the mirRNA miR-335 in its second intron. In particular we showed that forced down-regulation of miR-335 in AXL-negative cells was sufficient to increase the expression of AXL and to induce phenotypic and molecular features that are characteristic of AXL-positive cells, such as epithelial-to-mesenchymal transition and Erlotinib resistance.

Altogether these observations define a novel mechanism that couples epigenetic/stochastic inheritance to the ontogeny of the AXL-positive/Erlotinib-resistant cells. This novel framework could inform the development of novel cancer treatments based on the targeting of both AXL-negative and AXL-positive cell populations.

RESULTS

AXL-positive cells are pre-existing in cell lines and tumors

It has been shown that when non-small cell lung cancer (NSCLC)-derived cell lines harboring EGFR-oncogenic mutations are exposed to EGFR-TKIs like Erlotinib, populations of AXL-positive/Erlotinib-resistant cells emerge with features similar to those observed in tumors that have developed Erlotinib treatment resistance in patients (Zhang, Lee et al. 2012). This is the case for the NSCLC derived cell lines H1650-M3 and PC14. These cells are derivative of H1650 and PC9 cells respectively, harbor EGFR oncogenic mutations and were previously generated by culturing the parental cells with constant high concentrations of Erlotinib (Yao, Fenoglio et al. 2010).

We wondered if AXL-positive cells are present in tumors prior to treatment as well as in tumor derived cell lines and whether these cells bear phenotypic and molecular similarities to the AXL-positive cells that are generated upon exposure to EGFR-TKI (Zhang, Lee et al. 2012).

Given that AXL is a cell surface receptor, we utilized FACS sorting analysis with an antibody that recognizes an epitope localized within the N-terminal extra-cellular moiety of AXL to identify and separate putative AXL-positive cells. By using the AXL-positive cell lines, H1650-M3 and PC14 as reference (Figure 1A and B), we observed the presence of AXL-positive cells in multiple Erlotinib-naïve cell populations (Figure 1B-D). The presence of these AXL-positive cells was not restricted to tumor-derived cell lines harboring EGFR-oncogenic mutations, as we observed that a similar percentage of AXL-positive cells were present also in cell lines driven for example by mutant KRAS (i.e., A549)(Figure 1C-D).

In tumors, the expression of AXL is often accompanied by the expression of its ligand, GAS6 resulting in the constitutive activation of AXL and its downstream signaling pathways (i.e., AKT and ERK). We found that this was the case also in the pre-existing FACS-sorted AXL-positive

cells. Our RT-PCR and western-blot analysis confirmed the high expression of AXL and GAS6 in these cells (Figure 1D-F) and indicated that AXL as well as AKT were constitutively phosphorylated in AXL-positive cells (Figure 1F).

To exclude the possibility that our observations were an artifact of our cell culture system and more importantly to test the relevance of our findings in patients, we performed similar analyses in five primary NSCLC tumors. To limit our analysis only to tumor cells, we analyzed AXL expression only in cells that were $CD45^-$, $CD31^-$ and $EPCAM^{mid/high}$. This FACS algorithm excludes bone marrow derived cells, endothelial cells, and fibroblasts. Also in this case, we found that human primary drug-naïve tumors contained a subpopulation of cells with high expression of AXL and GAS6 (Figure 1G and H; Figure 1- figure supplement 1A).

Pre-existing AXL-positive cells have phenotypic and molecular features of Erlotinib-resistant cells

Having shown the existence of AXL-positive cell populations in primary tumors and in tumor derived cell lines, next we tested whether these cells had phenotypic and molecular features of Erlotinib resistant AXL-positive cells. We found that AXL-positive FACS-sorted cells from Erlotinib-naïve cell lines (i.e., PC9 AXL+ve) and AXL-positive cells that were generated upon Erlotinib-selection (i.e., PC14) had similar sensitivity to Erlotinib treatment with IC_{50} almost 3 times higher than parental cells (i.e., PC9) (Figure 2A). To further explore the role of AXL in adaptive resistance to TKI, we performed an Erlotinib and Gefitinib sensitivity assay with AXL-negative and positive cells mixed together in different ratios. We found that the presence of AXL-positive cells resulted in a significantly higher number of drug-resistant colonies, compared with only AXL-negative cells (Figure 2-figure supplement 1 A-B).

The FACS-sorted AXL-positive cells looked very similar to the AXL-positive cells that emerged following Erlotinib treatment (PC14 and H1650-M3). All possessed the morphological and molecular features of mesenchymal cells, including loss of cobblestone shape and increased stress fibers (Figure 2B and Figure2-figure supplement 1C) and differential expression of mesenchymal and epithelial markers (e.g., TGF-β1, TGF-β2, Slug, Twist, Vimentin and Zeb1) (Figure 2C; Figure 2-figure supplement 1D) (Zhang, Lee et al. 2012, Byers, Diao et al. 2013). These phenotypic features were driven by AXL because the inactivation of AXL in AXL-positive cells using the

pharmacological inhibitor BMS-777607 resulted in the loss of the mesenchymal marker Vimentin and increased expression of E-cadherin (Figure 2-figure supplement 1E).

Epithelial-to-mesenchymal transition can be induced by multiple cues, including the over-expression of certain receptor tyrosine kinase receptors like AXL, c-MET, PDGFR; exposure to TGF-β1, TGF-β2; or hypoxia (Yao, Fenoglio et al. 2010, Wu, Hou et al. 2013, Zhang, Huang et al. 2013, Rankin, Fuh et al. 2014, Elkabets, Pazarentzos et al. 2015, Li, Dobbins et al. 2015). Hence, we wondered whether the expression of AXL was a common feature of all mesenchymal cells or if on the contrary was specific to a particular cell state. Hence, we analyzed the presence of AXL-positive cells in multiple tumor derived cell lines and correlate their distribution with the mesenchymal status of the cells. Despite H1703, H1975 and H23 cells present with clear mesenchymal characteristics, AXL-positive cells were virtually absent in these cell lines (Figure 2-figure supplement 2A-C). Hence we concluded that while all mesenchymal cells share common characteristics such as increased stress fibers, increased motility, elongated shape, etc.; AXL-positive cells are a unique cell population with features that only partially overlap with other mesenchymal cells.

AXL-positive cells are generated stochastically

Cancer cells are characterized by intrinsic genetic instability that can give rise to clonal cell populations with distinctive genotypic and phenotypic qualities (Greaves and Maley 2012, Barber, Davies et al. 2015). In addition, it has been shown that intra-tumor heterogeneity could be spurred by non-genetic determinants (Polyak and Weinberg 2009, Meacham and Morrison 2013). In this regard, Gupta et al. have suggested that cancer cells can oscillate stochastically among different cell states characterized by differential expression of the surface markers CD44 and CD24 (Gupta, Fillmore et al. 2011). More recently, the Haber group also showed that circulating tumor cells from ER+/HER- patients can be HER2- and HER2+, and readily interconvert from one state to the other within 4 doubling times (Jordan, Bardia et al. 2016).

Here we tested if AXL-positive cells were generated stochastically. In fact, we reasoned that if the AXL-positive cells were generated by mutations, it would be very unlikely that these mutations would occur in synchrony. If this were the case, then we would expect the percentages of AXL-positive cells to vary across clonal cell lines derived from a single AXL-negative cell (Figure 3A). On the other hand, if the AXL-positive cells were generated through a stochastic event, we instead

would predict the percentages of AXL-positive cells to be similar in multiple clonal cell lines derived from a single AXL-negative cell (Figure 3B).

To explore these two models, we derived isogenic cell lines from FACS sorted AXL-negative H1650 and HCC827 cells; allowed them to expand; and then assessed the frequency of AXL-positive cells from four, single-cell derived clonal cell lines. We observed a very similar percentage of AXL-positive cells in the parental cells as well as in the single-cell derived clonal cell lines (Figure 3C-D; Figure 3-figure supplement 1A and B). Based on this finding, we concluded that AXL-positive cells are most likely generated from AXL-negative cells via a non-genetic, stochastic mechanism.

To further confirm this observation and to improve our understanding of the cell-state plasticity of AXL-positive and AXL-negative cells, we sorted pure AXL-positive and AXL-negative cells from the H1650 cell line and analyzed the distribution of AXL-positive and AXL-negative progeny of cells over time (Figure 3E). We found that within three weeks, the AXL-negative cells could regenerate cell populations with the same percentage of AXL-positive and AXL-negative cells as the parental cell line. Interestingly, we observed that even though the AXL-positive cells took a longer time to do so (18 weeks), they too were able to regenerate a progeny population with the same percentages of AXL-positive and AXL-negative as present in the parental cell line. To exclude the possibility that this finding was the result of competition among clones driven by genetic mutations, we repeated the same experiments using a single-cell derived cell line (e.g., H1650- clone 2). In this case, a nearly identical trend was recapitulated (Figure 3F).

miRNA profiling of AXL-positive cells revealed a unique miRNA signature

Among the many possible regulators of cell-state plasticity, we sought to investigate whether microRNAs (miRNAs) were involved in modulating the ontogeny of AXL-positive cells (Garzon, Marcucci et al. 2010).

miRNAs are small (~22 nt) non-coding RNAs constituting a novel class of gene regulators that post-transcriptionally repress gene expression by initiating the degradation or blocking translation of target mRNAs (Lau, Lim et al. 2001, Lee and Ambros 2001, Ambros, Bartel et al. 2003). More than 1000 unique, mature miRNAs have been identified in the human genome (Griffiths-Jones 2004) and each may regulate up to 200 mRNAs (Lewis, Shih et al. 2003, Betel, Wilson et al. 2008).

In fact, it is estimated that roughly 30% of all human gene transcripts are targeted by miRNAs, implicating them in the regulation of virtually all cellular processes.

We generated miRNA expression profiles from the AXL-positive H1650-M3 and parental AXL-negative H1650 cells by constructing small RNA libraries. These libraries were deep sequenced using the Illumina platform. Sequence reads were mapped to the human genome using a customized bioinformatics pipeline. Reads were annotated by BLAT (Kent 2002) to a unified database containing entries for human small RNAs from miRBase (Griffiths-Jones 2004), NONCODE (Liu, Bai et al. 2005), tRNAs in The RNA Modification Database (Limbach, Crain et al. 1994), and rRNA entries in the Entrez Nucleotide Database (Schuler, Epstein et al. 1996). Our previous experience performing comparative analysis informed our decision to use an arbitrary cut-off of a minimum of 1000 reads and >2 fold differential expression. Using these criteria, we identified 20 miRNAs that were up-regulated and 19 miRNAs that were down-regulated in the AXL-positive H1650-M3 cells compared to the AXL-negative H1650 cells (Figure 4A and B). Differential miRNA expression levels were independently validated by quantitative stem-loop RT-PCR (qRT-PCR) in the AXL-negative (H1650) and AXL-positive (H1650-M3) cell lines (Figure 4C). Apart from let7c, the differential miRNA expression patterns of all miRNAs identified by our deep sequencing analysis were confirmed (Figure 4C).

Although none of the identified miRNAs were predicted to target AXL, we were intrigued by the differential expression of miR-335 we observed in AXL-positive compared to AXL-negative cells. In fact, miR-335 has been reported to suppress a mesenchymal-like state and metastatic dissemination by targeting a diverse set of genes regulating cell migration, extra-cellular matrix remodeling, cell self-renewal and epigenetic reprograming (Tavazoie, Alarcon et al. 2008) (Figure 1D). Among them, of particular interest was the regulation of the TGF-β axis by miR-335. In fact, TGF-β is a well known regulator of AXL and AXL activity (Lynch, Fay et al. 2012). Furthermore, the TGF-β axis has also been shown to suppress the expression of multiple miRNAs that we found to be down-regulated in AXL-positive cells (Gregory, Bracken et al. 2011, Yang, Li et al. 2012, Kato, Dang et al. 2013). Altogether these findings let us to hypothesize that differentially expressed miRNAs in AXL-positive cells could be part of a hierarchically organized miRNA cluster primed by miR-335 and that the regulation of miR-335 could play a major role in the ontogeny of AXL-positive cells.

As a first step to test this possibility, we determined how general was the decreased in miR-335 expression we observed in AXL-positive cells. To this end, we examined the expressionof miR-335 in: 1) Erlotinib resistant H1650-M3 and PC14 cells (Figure 4E), 2) FACS sorted AXL-positive and AXL-negative cells from H1650 and HCC827 cell lines (Figure 4F), as well as 3) FACS sorted cells from four human primary NSCLC tumors (Figure 4G). In all these cases, when we measured the expression of miR-335 by qRT-PCR, we consistently found that miR-335 levels were decreased in all AXL-positive cells (Figure 4E-G).

To verify that miR-335 was active in AXL-positive cells, next, we compared the expression levels of known and predicted miR-335 targets. RT-PCR analysis showed that the miR-335 targets SOX4, TNC, COL1A1, PTPRN2, MERTK, PLCB1, LAMB2, FGF2, JAG1, BMI1, SMARCA2, MAX were expressed at higher levels in AXL-positive; miR-335 low cells (H1650-M3) compared to AXL-negative;miR-335 high cells (H1650) (Figure 4D).

We previously have shown that AXL-positive cells have an increased activation of the TGF-beta pathway (See figure 2). To determine if miR-335 was sufficient to regulate the activity of the TGF-β pathway, we inactivated miR-335 by transfecting AXL-negative cells with three independent Antagomirs and assessed the expression of TGF-β 1 and 2 and some of their down-stream targets (e.g., Vim, Ecadh, Snail) by RT-PCR. We found that the Antagomirs treatment decreased the expression of miR-335 (Figure 4-figure supplement 1A) and of its targets (Figure 4-figure supplement 1B) as well as of TGF-β 1/ 2 (Figure 4-figure supplement 1C) and of the TGF-β target genes VIM, Ecadh, SNAI, SLUG, etc. compared to control (Figure 5D).

As reported in the literature, we also observed the majority of miRNAs we observed to be differentially expressed in AXL-positive and AXL-negative cells to be regulated by TGF-β 1/ 2 except for MiR-335 (Figure 4H and I). Consistent with TGF-beta being regulated by miR-335, we also found that inactivation of miR-335 was sufficient to reduce the expression of these miRNAs (miR-20a, miR-34a, miR-200c, etc.) but to increase the expression of miR-143 and miR-195, which were expressed at higher levels in AXL-positive cells when compared to AXL-negative cells (Figure 4J).

miR-335 regulates the ontogeny of AXL-positive cells.

Our data indicated that miR-335 regulate the expression of key molecular determinant of the AXL-positive state. To test if miR-335 could regulate the ontogeny of AXL-positive cells, we decreased the expression of miR-335 using Antagomir treatment in multiple AXL-negative cells and analyzed the morphology, the expression of signature genes as well as their resistance to EFGR Tki.

We observed that treatment of AXL-negative cell lines (H1650 and PC9) with a miR-335 Antagomir resulted in a reduction of miR-335 expression (Figure 5A) and an increased expression of AXL-positive cells (Figure 5B; Figure 5-figure supplement 1A). This was accompanied by epithelial- to-mesenchymal transition manifested by loss of the classic cobblestone appearance of epithelial cells (Figure 5C) and changes in EMT molecular markers (Figure 5D).

In a standard drug sensitivity assay, we observed that treatment with miR-335 Antagomir also increased the cells resistance to Eroltinib treatment to levels similar to what we observed when we tested the AXL-positive cell lines we derived by Erlotinib selection (Figure 5 E and F).

To provide additional proof that inhibition of miR-335 was sufficient for the generation of AXL-positive cells, we utilized CRISPR-CAS9 gene editing as an orthogonal approach. Also in this case and consistent with our previous results, genetic inactivation of miR-335 resulted in the acquisition of phenotypic and molecular characteristics of AXL-positive cells (Figure 5-figure supplement 2A-C).

Altogether, these observations indicate that miR-335 serves as a critical regulator of the interconversion of AXL-negative and AXL-positive cell states beyond its well-studied role in the regulation of metastasis (Tavazoie, Alarcon et al. 2008).

Methylation of *MEST* isoform 2 promoter modulates miR-335 expression in AXL-positive cells

The miR-335 encoding sequence resides in the second intron of the *mesoderm-specific transcript homolog* (*MEST*)/*paternally expressed 1* (*PEG1*) gene located on chromosome 7q32. In humans, two distinct CpG islands have been identified in the promoters of *MEST* (Figure 6A) (Png, Yoshida et al. 2011, Dohi, Yasui et al. 2013). To investigate the possible epigenetic regulation of miR-335, we analyzed levels of *MEST* CpG island 1 and 2 methylation by bisulfite sequencing, methylation-

specific RT-PCR, as well as qRT-PCR in AXL-positive H1650-M3 and AXL-negative H1650 cells (Figure 6A and B). We found that although no significant differences were observed in the methylation of CpG island 2, CpG island 1 was differentially methylated in the AXL-positive H1650-M3 cells, and associated with higher expression of MEST isoform 1 and decreased expression of miR-335 (Figure 6B, Figure 6-figure supplement 1A).

We extended these analyses to include AXL FACS sorted cell lines (H1650 and PC9) and human NSCLC tumor-derived cells. Again, we found that all AXL-positive cells displayed an increased methylation of CpG island 1 relative to AXL-negative cells (Figure 6C and D; Figure 6-figure supplement 1B).

To establish the functional relevance of the hyper-methylation of the *MEST* isoform 2 promoter, we treated AXL-negative H1650 cells and AXL-positive H1650-M3 cells with the DNA methylation inhibitor 5-aza-2'-deoxycytidine (5-aza-dC) along with Trichlostatin A (TSA). We observed a dose-dependent change in the methylation of CpG island 1 and, consistent with the role of CpG island hyper-methylation in gene silencing, increased expression of miR-335 in AXL-positive cells (Figure 6E and F). Importantly, no differences were observed in the AXL-negative H1650 cells upon treatment with 5-aza-dC compared to the control. In accordance with the proposed role of miR-335 in the regulation of AXL, we also observed a decrease in AXL mRNA expression along with a decrease in the proportion of AXL-positive cells upon inhibiting DNA methylation with 5-Aza-dC (Figure 6G; Figure 6-figure supplement 1C). These changes were most likely due to increased miR-335 levels as inhibition of miR-335 by Antagomir treatment impeded the observed decrease in the number of AXL-positive cells in H1650-M3 cells (AXL-positive) treated by 5-aza-dC (Figure 6G).

To further characterize a possible role of miR-335/MEST DNA methyaltion in Erlotinib ressitance, we performed a drug sensitivity assay after pre-treating the cells with 5-Aza-dC. Consistent with 5-Aza-dC decreasing MEST promoter methylation and AXL expression in AXL-positive cells (Figure 6E-G), we observed a decreased in AXL-positive cells in H1650 cells upon 5-Aza-dC treatment (Figure 6-figure supplement 1D) and an increased sensitivity of cells to Erlotinib (Figure 6H).

Based on these observations, we concluded that differential miR-335 promoter methylation is responsible for the decreased expression of miR-335 observed in AXL-positive cells, and that the

375 transition between the AXL-positive and AXL-negative cell states as well as their differential
376 resistence to EGFR TKi is regulated epigenetically.
377

DISCUSSION

Drug resistance continues to be a major hurdle that oncologists face in treating cancer patients. Although the genetic diversity of tumors has been proposed to drive the acquisition of drug resistance; emerging data indicate that also non-genetic determinants could be equally significant (Brock, Chang et al. 2009). These include the interaction of a tumor with its micro-environment as well as the occurrence of cell-intrinsic molecular mechanisms such as epigenetic changes (Brock, Chang et al. 2009, Muranen, Selfors et al. 2012).

In the case of lung tumors driven by oncogenic-EFGR mutations, it has been observed that approximately 15% of tumors that become resistant to EGFR TKi are characterized by mesenchymal like features and higher expression of AXL. In these tumors inhibition of AXL restore the sensitivity to EGFR TKi (Zhang, Lee et al. 2012). In contrast to other mechanisms of resistance to EGFR TKi, in these tumor cells AXL was neither mutated, amplified or its expression driven by EGFR TKi treatment as in the case of the persistent cells originally described by Settleman et al. (Sharma, Lee et al. 2010).

Here we described a novel molecular mechanism driving the ontogeny of AXL-positive EGFR TKi resistant cells based on the stochastically fluctuation of cancer cells between an AXL-negative state characterized by epithelial-like features and an AXL-positive state in which cells are mesenchymal and have an increased resistance to EGFR TKi (Figure 7). The switch between these two cell-states is restricted by miR-335 as all AXL-positive cells we examined were characterized by a decreased expression of miR-335 and that inactivation of miR-335 decreased the number of AXL-positive cells and reverted AXL-positive cells into AXL-negative cells.

Although miR-335 restricts the transition of AXL-positive into AXL-negative cells, AXL mRNA does not contain a miR-335 seeding sequence, which means it is unlikely to be a direct target of miR-335. Yet, miR-335 has been previously shown to regulate the expression of a multitude of signaling pathways including components of the TGF-β axis. The regulation of the TGF-β axis by miR-335 is of particular interest because AXL is a known downstream target of TGF-β; hence suggesting a possible molecular linking AXL and miR-335 (Bauer, Zagorska et al. 2012).

The inhibition of the TGF-β signaling pathway by miR-335 is particularly interesting also because exposure to TGF-β regulate the expression of several of the miRNAs associated with the AXL-

positive state, such as miR-20a, miR-34a, miR-200c, etc. Among them of particular significance were the mir-200 family members, as they not only induce EMT but also resistance to Erlotinib (Brabletz and Brabletz 2010).

Lastly, miR-335 is among approximately 50 miRNAs that are regulated epigenetically by DNA methylation of CpG islands within promoter regions (Lujambio and Esteller 2007). The epigenetic regulation of miR335 is particularly interesting in light of the observation that AXL-positive and AXL-negative cell populations are highly dynamic. AXL FACS-sorted cells can in fact interconvert until the same two cell states distribution observed in the parental cell population is reached (Figure 3E). Notably, we observed the time required for AXL-positive and AXL-negative cell populations to reach equilibrium is different. While within a few weeks the AXL-negative cells generated a population of cells with the same distribution of AXL-positive and AXL-negative cells as was observed in the parental cell line; it took the AXL-positive cells a couple of months to reach this equilibrium. At this time, we don't have a clear molecular mechanism explaining these differences, yet it is tentative to hypothesize that --given the stochastic regulation of miR335-- because the AXL-positive cells grow slower than AXL-negative cells, it will take longer time for the former to switch state. Alternatively, it is tempting to postulate that the inter-conversion between the two cell states could be regulated by enzymatic activities occurring at different rates. This hypothesis is informed by the possibility that the de-methylation rate of the CpG1 on the miR-335 promoter could occur less efficiently than its methylation.

One important feature of AXL-positive cells is their intrinsic resistance to EGFR TKi. This implies that because AXL-postive cells could revert back to an AXL-negative state, the drug resistance observed in AXL-positive tumors, although heritable, is not a stable trait in the population. Consequently, as shown in the schematic in Figure 7, AXL-negative cells could hypothetically emerge over time following drug removal. This phenomenon is in principle similar to the observation that certain Erlotinib-resistant tumors expressing neuroendocrine markers can revert to an epithelial-like state over time upon interruption of the drug treatment (Niederst, Sequist et al. 2015).

Nevertheless, the AXL-positive cells that survived to the drug treatment can accumulate novel genetic mutations that can alter the innate equilibrium between AXL-positive and AXL-negative, and, consequently, produce tumors that are stable AXL-positive state (Figure 7). This explanation seems to hold true for certain clonal populations, including the H1650-M3 and PC14 cells that were

446 selected to grow and expand in the presence of high Erlotinib concentrations. In fact, these cell
447 lines maintain features associated with the AXL-positive cell state even in the absence of drug
448 treatment. Interestingly, we have recently observed that TGF-beta by repressing DNA repair could
449 spur the accumulation of mutations and accelerate the clonal evolution of tumors (Pal, Pertot et al.
450 2017). These findings have important clinical implications. They in fact predict that treatments
451 based only on targeting the epithelial, AXL-negative cells will be insufficient and destine to fail.
452

MATERIALS AND METHODS

Cell culture

H1650, HCC4006, HCC827, A549, H358 and H2228 cell lines were purchased from American Type Culture Collection. All cell lines were authenticated through Short Tandem Repeat (STR) profiling and regularly tested for mycoplasma. H1650-M3 was generated by culturing H1650 cell line in the presence of a constant high concentration of Erlotinib. All cell lines were maintained in RPMI GlutaMAX (Invitrogen) containing 5% Fetal Bovine Serum. Medium was supplemented with 100 units/ml of penicillin and 100 ug/ml of Streptomycin (Invitrogen). All cell lines were cultured at 37^{o}C and 5% CO_2.

Generation of isogenic clones:

H1650 cells were serially diluted in 96 wells such that one well contains one cell. They were then grown for 2 months before the experiments.

TGF-β treatment

Cells were treated with rhTGFβ1 and rhTGFβ2 (R&D systems, Minneapolis, MN) 1 ng/ml each in complete media, for 72 hrs. Following treatment, the cells were harvested for RNA preparation and qRT-PCR, for immunoblotting or for cell cycle analysis.

TGF-β inhibitor treatment

For treatment with LY2157299 (20 μM) (TGFBR1 kinase inhibitor, Selleckchem, Houston, TX), 300,000 H1650-M3 cells were plated in a 6 cm^2 plate. Inhibitor was added the next day and the mixture was incubated for 3–5 days for LY2157299. The cells were lysed with TRIzol and processed for RNA preparation.

Drug treatment

To determine IC50 values for various drugs (Erlotinib and BMS-777607), the cells were plated in 96-well plates at 1000 cells/well. The next day, individual drugs were added to the wells at the indicated concentrations and incubated for 5 days. The plates were then washed once with PBS, fixed with 3.7% formaldehyde and stained with Crystal violet. Each stained well was destained in 50-100 μl of 10% acetic acid and the absorbance was read in a spectrophotometer at 590 nm.

Long term drug treatment to generate persisters

RNAi Transfection, RNA extraction and quantitative Real-Time PCR

RNAi transfection was performed using Lipofectamine™ 2000 (Invitrogen) as per manufacturer's protocol. Unless otherwise indicated, total RNA was collected 72 hours after transfection. Total RNA was extracted using Trizol (Life technologies). Removal of contaminating genomic DNA was performed by incubation with RQ1 RNase-Free DNase (Promega) for 30 min. 1000ng total RNA was reverse transcribed using ImProm-II reverse transcriptase and Oligo-dT primers. Quantitative PCR was carried out using Power SYBR Green PCR master mix on a 7900HT Fast Real-Time System (Applied Biosystems) or QuantStudio-6 Real-Time System (Applied Biosystems). Power SYBR Green Cells-to-Ct kit was used to perform quantitative PCR on 10,000 cells sorted from tumors. Analyses were done in triplicate and Actin or GAPDH were used as a reference gene. A complete list of primer sequences is supplied in Supplementary file 1.

miRNA analysis

Total RNA was extracted using miRCURY™RNA isolation kit- cell & plant (Exiqon) according to manufacturer's instructions. On-column removal of genomic DNA was performed using RQ1 RNase-Free DNase (Promega). cDNA synthesis was performed using miRCURY LNA Universal RT microRNA PCR, Polyadenylation and cDNA synthesis kit (Exiqon; 203300) and miRCURY LNA Universal RT microRNA PCR SYBR green master mix was used for quantitative real-time PCR analysis. U6 snRNA was used as reference gene. A complete list of primer sequences is supplied in Supplementary file 1.

Methylation specific RT-PCR, QPCR and bisulfite sequencing

1 µg genomic DNA was pretreated with sodium hydroxide for 15 minutes at 37 ^{o}C followed by incubation with hydroquinone (Sigma) and sodium metabisulfite (Sigma) for 16 hours at 50^{o}C. The busilfite modified DNA was subsequently purified using Wizard DNA Clean-up system (Promega). Genomic DNA from in vitro methylated Jurkat cells were (Active Motif) served as positive control and genomic DNA from H1993 cells served as negative control. RT-PCR analysis was performed using Immolase DNA polymerase (Bioline) and fragments were separated on 2% argarose gels. Takara Episcope MSP kit was used for performing quantitative RT-PCR on a 7900HT Fast Real-Time System (Applied Biosystems). For analysis by bisulfite sequencing, fragments were cloned into the pGEM®-T Easy Vector (Promega) and 20 colonies from each sample were sequenced. A complete list of primer sequences is supplied in Supplementary file 1.

Immunofluorescence

AXL –ve and AXL-positive cells from H1650 and PC9 were FACS-sorted and cultured for 2 days in an 8-well chamber slide system (LAB-TEK, Thermo Fisher Scientific). H1650, H1650-M3, PC9 and PC14 cells were grown on glass coverslips in a 24-well Petri dish. Cells were fixed with 4% para-formaldehyde and permeabilized in 0.1% Triton X-100 in PBS for 10 minutes. Fixed cells were washed three times in PBS and blocked with 1% BSA in PBS for 1 hour. After washing three times with PBS, the cells were incubated with Alexa-Fluor 488 Phalloidin for 30 min at room temperature. DAPI was used for nuclear staining. The stained cells were mounted with a Vectashield mounting medium (Vector Laboratories, Burlingame, California) and analyzed using a confocal microscope.

Immunoprecipitation and Western Blot Analysis

Total cell lysates were obtained by lysing cells in modified denaturing buffer (50mM Tris-Cl pH 7.5, 1 mM EDTA, 1 mM EGTA 1% Triton-X, 0.27M Sucrose, 1% β-mercaptoethanol) with protease inhibitor tablets and phosphatase inhibitors (10mM NaF, 1mM PMSF, 1mM Na_3VO_4). Lysate were incubated on ice for 30 min, mixed end-to-end at 4C for 30 min and then centrifuged at 13,000g for 30 min to remove debri. 1500 µg total protein lysate was 100ul slurry of pre-cleared with Protein G agarose beads (Promega), followed by overnight incubation with AXL antibody (2ug Ab/ 100 ul lysate). Immunocomplexes were pulled down by incubating with 100ul slurry of pre-cleared with Protein G agarose beads. Immunoprecipitation complex and 10% lysate inputs were separated on 8% polyacrylamide gels, transferred to nitrocellulose membrane and blotted overnight with antibody against AXL, Phospho-AXL, Phospho-Tyrosine. β-tubulin was used was used as loading control.

Flow cytometry

Cells were dissociated using TrypLE (Invitrogen) and washed with cold PBS containing 5% Fetal Bovine Serum. Resuspended cells were filtered through a 40 micron mesh to generate single cell suspension and incubated with directly conjugated fluorescent antibodies to the desired antigens for 20 minutes on ice in the dark and subsequently washed 3 times with cold PBS pH 7.2. Analysis of AXL-negative and AXL-positive cell populations was performed on the LSRII (BD Biosciences). A total of 20,000 cells were analyzed using the FACSDiva 6.0 software (BD Biosciences). Isolation of AXL-negative and AXL-positive cells were done by Fluorescent Activated Cell Sorting performed on the Aria II (BD Biosciences). For sorting cells from tumor, we stained a single-cell suspension derived from tumors with CD45, CD31, EpCAM and AXL

antibodies. Based on the isotype staining, we gated the CD45-/ CD31-/ EpCAM $^{mid/high}$ population and then gated the desired AXL-negative and AXL-positive populations from the EpCAM $^{mid/high}$ population.

Statistical analysis

Data are represented as mean ± SD. Statistical analysis of experimental data were conducted using GraphPad Prism 7.0 software (San Diego, CA, USA). Student's t-test (two tailed) was used for two group comparisons. Spearman's rank test was used to measure correlation between two variables. $P< 0.05$ was considered statistically significant.

Patient Study Details:

The collection of human lung tissue samples and blood for this study was covered by Northwell Health/ Cold Spring Harbor Laboratory IRB #TDP-TAP 1607 (Raffaella Sordella/10/11/16). The samples were acquired from patients already undergoing thoracic procedures (e.g. surgical tumor resection, biopsy) at Huntington Hospital. All study participants provided informed consent for the use of their lung tissue and blood for research purposes. Participants were informed of study aims, the potential risks and benefits of participation, and that any discoveries facilitated by the analysis of their tissues might be published. The participants were informed that their names would not be associated their samples in any publication or presentation of research findings.

Reagents

Recombinant human TGF-β1 and TGF-β2 was purchased from R&D Systems. miR-335 antagomirs were obtained from the following companies: antagomir 1 from Ambion; antagomir 2 from Exiqon (miRCURY LNA microRNA Power Inhibitor; 4100464-002) and antagomir 3 from Thermo Scientific Dharmacon (miRIDIAN hairpin inhibitor; IH-300708-07). miR-335 Mimic oligonucleotide was obtained from Exiqon (473600-001). The following chemical reagents were used for cell treatment: Erlotinib Hydrochloride 99% from LGM Pharmaceutical Inc, pyridone 6 (P6) from Calbiochem, Trichlostatin (TSA) and 5-aza-2-deoxycytidine from Sigma-Aldrich.

Antibodies

For Flow Cytometry

APC anti-human AXL antibody (R & D Systems); cat # FAB154A

Alexa Fluor 488 anti-human AXL

PE-CF594 anti-human CD45 antibody (BD Biosciences); cat. # 562279

BV421 anti-human CD31 antibody (BD Biosciences); cat # 564089

Alexa Fluor 488 anti-human CD326 (Ep-CAM) antibody (BioLegend); cat # 324210

For Immunofluorescence

Alexa Fluor 488 Phalloidin (Thermo Fisher)

For Immunoprecipitation and Immunoblot analysis

AXL M-20 goat polyclonal IgG (SCBT); cat. # sc-1097. Currently discontinued.

Anti-alpha-tubulin antibody (Millipore) cat. # MABT205

Phospho- Tyr PY20 mouse monoclonal IgG (SCBT); cat. # sc-508

Phospho-AXL mouse monoclonal IgG (R & D Biosystems); cat. #

Gas6

GAPDH

Ras-GAP

REFERENCES

Ambros, V., B. Bartel, D. P. Bartel, C. B. Burge, J. C. Carrington, X. Chen, G. Dreyfuss, S. R. Eddy, S. Griffiths-Jones, M. Marshall, M. Matzke, G. Ruvkun and T. Tuschl (2003). "A uniform system for microRNA annotation." RNA **9**(3): 277-279.

Barber, L. J., M. N. Davies and M. Gerlinger (2015). "Dissecting cancer evolution at the macro-heterogeneity and micro-heterogeneity scale." Curr Opin Genet Dev **30**: 1-6.

Bauer, T., A. Zagorska, J. Jurkin, N. Yasmin, R. Koffel, S. Richter, B. Gesslbauer, G. Lemke and H. Strobl (2012). "Identification of Axl as a downstream effector of TGF-beta1 during Langerhans cell differentiation and epidermal homeostasis." J Exp Med **209**(11): 2033-2047.

Bean, J., C. Brennan, J. Y. Shih, G. Riely, A. Viale, L. Wang, D. Chitale, N. Motoi, J. Szoke, S. Broderick, M. Balak, W. C. Chang, C. J. Yu, A. Gazdar, H. Pass, V. Rusch, W. Gerald, S. F. Huang, P. C. Yang, V. Miller, M. Ladanyi, C. H. Yang and W. Pao (2007). "MET amplification occurs with or without T790M mutations in EGFR mutant lung tumors with acquired resistance to gefitinib or erlotinib." Proc Natl Acad Sci U S A **104**(52): 20932-20937.

Bell, D. W., I. Gore, R. A. Okimoto, N. Godin-Heymann, R. Sordella, R. Mulloy, S. V. Sharma, B. W. Brannigan, G. Mohapatra, J. Settleman and D. A. Haber (2005). "Inherited susceptibility to lung cancer may be associated with the T790M drug resistance mutation in EGFR." Nat Genet **37**(12): 1315-1316.

Ben-Batalla, I., A. Schultze, M. Wroblewski, R. Erdmann, M. Heuser, J. S. Waizenegger, K. Riecken, M. Binder, D. Schewe, S. Sawall, V. Witzke, M. Cubas-Cordova, M. Janning, J. Wellbrock, B. Fehse, C. Hagel, J. Krauter, A. Ganser, J. B. Lorens, W. Fiedler, P. Carmeliet, K. Pantel, C. Bokemeyer and S. Loges (2013). "Axl, a prognostic and therapeutic target in acute myeloid leukemia mediates paracrine crosstalk of leukemia cells with bone marrow stroma." Blood **122**(14): 2443-2452.

Betel, D., M. Wilson, A. Gabow, D. S. Marks and C. Sander (2008). "The microRNA.org resource: targets and expression." Nucleic Acids Res **36**(Database issue): D149-153.

Brabletz, S. and T. Brabletz (2010). "The ZEB/miR-200 feedback loop--a motor of cellular plasticity in development and cancer?" EMBO Rep **11**(9): 670-677.

Braunger, J., L. Schleithoff, A. S. Schulz, H. Kessler, R. Lammers, A. Ullrich, C. R. Bartram and J. W. Janssen (1997). "Intracellular signaling of the Ufo/Axl receptor tyrosine kinase is mediated mainly by a multi-substrate docking-site." Oncogene **14**(22): 2619-2631.

Brock, A., H. Chang and S. Huang (2009). "Non-genetic heterogeneity--a mutation-independent driving force for the somatic evolution of tumours." Nat Rev Genet **10**(5): 336-342.

Brose, M. S., P. Volpe, M. Feldman, M. Kumar, I. Rishi, R. Gerrero, E. Einhorn, M. Herlyn, J. Minna, A. Nicholson, J. A. Roth, S. M. Albelda, H. Davies, C. Cox, G. Brignell, P. Stephens, P. A. Futreal, R. Wooster, M. R. Stratton and B. L. Weber (2002). "BRAF and RAS mutations in human lung cancer and melanoma." Cancer Res **62**(23): 6997-7000.

Byers, L. A., L. Diao, J. Wang, P. Saintigny, L. Girard, M. Peyton, L. Shen, Y. Fan, U. Giri, P. K. Tumula, M. B. Nilsson, J. Gudikote, H. Tran, R. J. Cardnell, D. J. Bearss, S. L. Warner, J. M. Foulks, S. B. Kanner, V. Gandhi, N. Krett, S. T. Rosen, E. S. Kim, R. S. Herbst, G. R.

649 Blumenschein, J. J. Lee, S. M. Lippman, K. K. Ang, G. B. Mills, W. K. Hong, J. N. Weinstein,
650 Wistuba, II, K. R. Coombes, J. D. Minna and J. V. Heymach (2013). "An epithelial-
651 mesenchymal transition gene signature predicts resistance to EGFR and PI3K
652 inhibitors and identifies Axl as a therapeutic target for overcoming EGFR inhibitor
653 resistance." Clin Cancer Res **19**(1): 279-290.
654 Dohi, O., K. Yasui, Y. Gen, H. Takada, M. Endo, K. Tsuji, C. Konishi, N. Yamada, H.
655 Mitsuyoshi, N. Yagi, Y. Naito, S. Tanaka, S. Arii and T. Yoshikawa (2013). "Epigenetic
656 silencing of miR-335 and its host gene MEST in hepatocellular carcinoma." Int J Oncol
657 **42**(2): 411-418.
658 Elkabets, M., E. Pazarentzos, D. Juric, Q. Sheng, R. A. Pelossof, S. Brook, A. O. Benzaken,
659 J. Rodon, N. Morse, J. J. Yan, M. Liu, R. Das, Y. Chen, A. Tam, H. Wang, J. Liang, J. M.
660 Gurski, D. A. Kerr, R. Rosell, C. Teixido, A. Huang, R. A. Ghossein, N. Rosen, T. G. Bivona,
661 M. Scaltriti and J. Baselga (2015). "AXL mediates resistance to PI3Kalpha inhibition
662 by activating the EGFR/PKC/mTOR axis in head and neck and esophageal squamous
663 cell carcinomas." Cancer Cell **27**(4): 533-546.
664 Engelman, J. A., T. Mukohara, K. Zejnullahu, E. Lifshits, A. M. Borras, C. M. Gale, G. N.
665 Naumov, B. Y. Yeap, E. Jarrell, J. Sun, S. Tracy, X. Zhao, J. V. Heymach, B. E. Johnson, L.
666 C. Cantley and P. A. Janne (2006). "Allelic dilution obscures detection of a biologically
667 significant resistance mutation in EGFR-amplified lung cancer." J Clin Invest **116**(10):
668 2695-2706.
669 Garzon, R., G. Marcucci and C. M. Croce (2010). "Targeting microRNAs in cancer:
670 rationale, strategies and challenges." Nat Rev Drug Discov **9**(10): 775-789.
671 Ghosh, A. K., C. Secreto, J. Boysen, T. Sassoon, T. D. Shanafelt, D. Mukhopadhyay and N.
672 E. Kay (2011). "The novel receptor tyrosine kinase Axl is constitutively active in B-
673 cell chronic lymphocytic leukemia and acts as a docking site of nonreceptor kinases:
674 implications for therapy." Blood **117**(6): 1928-1937.
675 Greaves, M. and C. C. Maley (2012). "Clonal evolution in cancer." Nature **481**(7381):
676 306-313.
677 Gregory, P. A., C. P. Bracken, E. Smith, A. G. Bert, J. A. Wright, S. Roslan, M. Morris, L.
678 Wyatt, G. Farshid, Y. Y. Lim, G. J. Lindeman, M. F. Shannon, P. A. Drew, Y. Khew-Goodall
679 and G. J. Goodall (2011). "An autocrine TGF-beta/ZEB/miR-200 signaling network
680 regulates establishment and maintenance of epithelial-mesenchymal transition." Mol
681 Biol Cell **22**(10): 1686-1698.
682 Griffiths-Jones, S. (2004). "The microRNA Registry." Nucleic Acids Res **32**(Database
683 issue): D109-111.
684 Gupta, P. B., C. M. Fillmore, G. Jiang, S. D. Shapira, K. Tao, C. Kuperwasser and E. S.
685 Lander (2011). "Stochastic state transitions give rise to phenotypic equilibrium in
686 populations of cancer cells." Cell **146**(4): 633-644.
687 Haber, D. A., D. W. Bell, R. Sordella, E. L. Kwak, N. Godin-Heymann, S. V. Sharma, T. J.
688 Lynch and J. Settleman (2005). "Molecular targeted therapy of lung cancer: EGFR
689 mutations and response to EGFR inhibitors." Cold Spring Harb Symp Quant Biol **70**:
690 419-426.
691 Jordan, N. V., A. Bardia, B. S. Wittner, C. Benes, M. Ligorio, Y. Zheng, M. Yu, T. K.
692 Sundaresan, J. A. Licausi, R. Desai, R. M. O'Keefe, R. Y. Ebright, M. Boukhali, S. Sil, M. L.
693 Onozato, A. J. Iafrate, R. Kapur, D. Sgroi, D. T. Ting, M. Toner, S. Ramaswamy, W. Haas,

694 S. Maheswaran and D. A. Haber (2016). "HER2 expression identifies dynamic
695 functional states within circulating breast cancer cells." Nature **537**(7618): 102-106.
696 Kabraji, S., X. Sole, Y. Huang, C. Bango, M. Bowden, A. Bardia, D. Sgroi, M. Loda and S.
697 Ramaswamy (2017). "AKT1low quiescent cancer cells persist after neoadjuvant
698 chemotherapy in triple negative breast cancer." Breast Cancer Res **19**(1): 88.
699 Kato, M., V. Dang, M. Wang, J. T. Park, S. Deshpande, S. Kadam, A. Mardiros, Y. Zhan, P.
700 Oettgen, S. Putta, H. Yuan, L. Lanting and R. Natarajan (2013). "TGF-beta induces
701 acetylation of chromatin and of Ets-1 to alleviate repression of miR-192 in diabetic
702 nephropathy." Sci Signal **6**(278): ra43.
703 Kent, W. J. (2002). "BLAT--the BLAST-like alignment tool." Genome Res **12**(4): 656-
704 664.
705 Lau, N. C., L. P. Lim, E. G. Weinstein and D. P. Bartel (2001). "An abundant class of tiny
706 RNAs with probable regulatory roles in Caenorhabditis elegans." Science **294**(5543):
707 858-862.
708 Lee, R. C. and V. Ambros (2001). "An extensive class of small RNAs in Caenorhabditis
709 elegans." Science **294**(5543): 862-864.
710 Lewis, B. P., I. H. Shih, M. W. Jones-Rhoades, D. P. Bartel and C. B. Burge (2003).
711 "Prediction of mammalian microRNA targets." Cell **115**(7): 787-798.
712 Li, W., S. Dobbins, I. Tomlinson, R. Houlston, D. K. Pal and L. J. Strug (2015).
713 "Prioritizing rare variants with conditional likelihood ratios." Hum Hered **79**(1): 5-
714 13.
715 Limbach, P. A., P. F. Crain and J. A. McCloskey (1994). "Summary: the modified
716 nucleosides of RNA." Nucleic Acids Res **22**(12): 2183-2196.
717 Liu, C., B. Bai, G. Skogerbo, L. Cai, W. Deng, Y. Zhang, D. Bu, Y. Zhao and R. Chen (2005).
718 "NONCODE: an integrated knowledge database of non-coding RNAs." Nucleic Acids
719 Res **33**(Database issue): D112-115.
720 Lujambio, A. and M. Esteller (2007). "CpG island hypermethylation of tumor
721 suppressor microRNAs in human cancer." Cell Cycle **6**(12): 1455-1459.
722 Lynch, J., J. Fay, M. Meehan, K. Bryan, K. M. Watters, D. M. Murphy and R. L. Stallings
723 (2012). "MiRNA-335 suppresses neuroblastoma cell invasiveness by direct targeting
724 of multiple genes from the non-canonical TGF-beta signalling pathway."
725 Carcinogenesis **33**(5): 976-985.
726 Lynch, T. J., D. W. Bell, R. Sordella, S. Gurubhagavatula, R. A. Okimoto, B. W. Brannigan,
727 P. L. Harris, S. M. Haserlat, J. G. Supko, F. G. Haluska, D. N. Louis, D. C. Christiani, J.
728 Settleman and D. A. Haber (2004). "Activating mutations in the epidermal growth
729 factor receptor underlying responsiveness of non-small-cell lung cancer to gefitinib."
730 N Engl J Med **350**(21): 2129-2139.
731 Mark, M. R., J. Chen, R. G. Hammonds, M. Sadick and P. J. Godowsk (1996).
732 "Characterization of Gas6, a member of the superfamily of G domain-containing
733 proteins, as a ligand for Rse and Axl." J Biol Chem **271**(16): 9785-9789.
734 Meacham, C. E. and S. J. Morrison (2013). "Tumour heterogeneity and cancer cell
735 plasticity." Nature **501**(7467): 328-337.
736 Muranen, T., L. M. Selfors, D. T. Worster, M. P. Iwanicki, L. Song, F. C. Morales, S. Gao,
737 G. B. Mills and J. S. Brugge (2012). "Inhibition of PI3K/mTOR leads to adaptive
738 resistance in matrix-attached cancer cells." Cancer Cell **21**(2): 227-239.

739 Nagata, K., K. Ohashi, T. Nakano, H. Arita, C. Zong, H. Hanafusa and K. Mizuno (1996).
740 "Identification of the product of growth arrest-specific gene 6 as a common ligand for
741 Axl, Sky, and Mer receptor tyrosine kinases." J Biol Chem **271**(47): 30022-30027.
742 Niederst, M. J., L. V. Sequist, J. T. Poirier, C. H. Mermel, E. L. Lockerman, A. R. Garcia, R.
743 Katayama, C. Costa, K. N. Ross, T. Moran, E. Howe, L. E. Fulton, H. E. Mulvey, L. A.
744 Bernardo, F. Mohamoud, N. Miyoshi, P. A. VanderLaan, D. B. Costa, P. A. Janne, D. R.
745 Borger, S. Ramaswamy, T. Shioda, A. J. Iafrate, G. Getz, C. M. Rudin, M. Mino-Kenudson
746 and J. A. Engelman (2015). "RB loss in resistant EGFR mutant lung adenocarcinomas
747 that transform to small-cell lung cancer." Nat Commun **6**: 6377.
748 O'Bryan, J. P., R. A. Frye, P. C. Cogswell, A. Neubauer, B. Kitch, C. Prokop, R. Espinosa,
749 3rd, M. M. Le Beau, H. S. Earp and E. T. Liu (1991). "axl, a transforming gene isolated
750 from primary human myeloid leukemia cells, encodes a novel receptor tyrosine
751 kinase." Mol Cell Biol **11**(10): 5016-5031.
752 Paez, J. G., P. A. Janne, J. C. Lee, S. Tracy, H. Greulich, S. Gabriel, P. Herman, F. J. Kaye, N.
753 Lindeman, T. J. Boggon, K. Naoki, H. Sasaki, Y. Fujii, M. J. Eck, W. R. Sellers, B. E. Johnson
754 and M. Meyerson (2004). "EGFR mutations in lung cancer: correlation with clinical
755 response to gefitinib therapy." Science **304**(5676): 1497-1500.
756 Pal, D., A. Pertot, N. H. Shirole, Z. Yao, N. Anaparthy, T. Garvin, H. Cox, K. Chang, F.
757 Rollins, J. Kendall, L. Edwards, V. A. Singh, G. C. Stone, M. C. Schatz, J. Hicks, G. J. Hannon
758 and R. Sordella (2017). "TGF-beta reduces DNA ds-break repair mechanisms to
759 heighten genetic diversity and adaptability of CD44+/CD24- cancer cells." Elife **6**.
760 Pillai, R. N. and S. S. Ramalingam (2012). "The biology and clinical features of non-
761 small cell lung cancers with EML4-ALK translocation." Curr Oncol Rep **14**(2): 105-
762 110.
763 Png, K. J., M. Yoshida, X. H. Zhang, W. Shu, H. Lee, A. Rimner, T. A. Chan, E. Comen, V. P.
764 Andrade, S. W. Kim, T. A. King, C. A. Hudis, L. Norton, J. Hicks, J. Massague and S. F.
765 Tavazoie (2011). "MicroRNA-335 inhibits tumor reinitiation and is silenced through
766 genetic and epigenetic mechanisms in human breast cancer." Genes Dev **25**(3): 226-
767 231.
768 Polyak, K. and R. A. Weinberg (2009). "Transitions between epithelial and
769 mesenchymal states: acquisition of malignant and stem cell traits." Nat Rev Cancer
770 **9**(4): 265-273.
771 Prasad, D., C. V. Rothlin, P. Burrola, T. Burstyn-Cohen, Q. Lu, P. Garcia de Frutos and G.
772 Lemke (2006). "TAM receptor function in the retinal pigment epithelium." Mol Cell
773 Neurosci **33**(1): 96-108.
774 Rankin, E. B., K. C. Fuh, L. Castellini, K. Viswanathan, E. C. Finger, A. N. Diep, E. L.
775 LaGory, M. S. Kariolis, A. Chan, D. Lindgren, H. Axelson, Y. R. Miao, A. J. Krieg and A. J.
776 Giaccia (2014). "Direct regulation of GAS6/AXL signaling by HIF promotes renal
777 metastasis through SRC and MET." Proc Natl Acad Sci U S A **111**(37): 13373-13378.
778 Samuels, Y., Z. Wang, A. Bardelli, N. Silliman, J. Ptak, S. Szabo, H. Yan, A. Gazdar, S. M.
779 Powell, G. J. Riggins, J. K. Willson, S. Markowitz, K. W. Kinzler, B. Vogelstein and V. E.
780 Velculescu (2004). "High frequency of mutations of the PIK3CA gene in human
781 cancers." Science **304**(5670): 554.
782 Schuler, G. D., J. A. Epstein, H. Ohkawa and J. A. Kans (1996). "Entrez: molecular
783 biology database and retrieval system." Methods Enzymol **266**: 141-162.

784 Sharma, S. V., D. Y. Lee, B. Li, M. P. Quinlan, F. Takahashi, S. Maheswaran, U.
785 McDermott, N. Azizian, L. Zou, M. A. Fischbach, K. K. Wong, K. Brandstetter, B. Wittner,
786 S. Ramaswamy, M. Classon and J. Settleman (2010). "A chromatin-mediated
787 reversible drug-tolerant state in cancer cell subpopulations." Cell **141**(1): 69-80.
788 Shaw, A. T. and J. A. Engelman (2016). "Crizotinib Resensitization by Compound
789 Mutation." N Engl J Med **374**(18): 1790-1791.
790 Shaw, A. T., B. Y. Yeap, M. Mino-Kenudson, S. R. Digumarthy, D. B. Costa, R. S. Heist, B.
791 Solomon, H. Stubbs, S. Admane, U. McDermott, J. Settleman, S. Kobayashi, E. J. Mark, S.
792 J. Rodig, L. R. Chirieac, E. L. Kwak, T. J. Lynch and A. J. Iafrate (2009). "Clinical features
793 and outcome of patients with non-small-cell lung cancer who harbor EML4-ALK." J
794 Clin Oncol **27**(26): 4247-4253.
795 Stephens, P., C. Hunter, G. Bignell, S. Edkins, H. Davies, J. Teague, C. Stevens, S. O'Meara,
796 R. Smith, A. Parker, A. Barthorpe, M. Blow, L. Brackenbury, A. Butler, O. Clarke, J. Cole,
797 E. Dicks, A. Dike, A. Drozd, K. Edwards, S. Forbes, R. Foster, K. Gray, C. Greenman, K.
798 Halliday, K. Hills, V. Kosmidou, R. Lugg, A. Menzies, J. Perry, R. Petty, K. Raine, L.
799 Ratford, R. Shepherd, A. Small, Y. Stephens, C. Tofts, J. Varian, S. West, S. Widaa, A.
800 Yates, F. Brasseur, C. S. Cooper, A. M. Flanagan, M. Knowles, S. Y. Leung, D. N. Louis, L.
801 H. Looijenga, B. Malkowicz, M. A. Pierotti, B. Teh, G. Chenevix-Trench, B. L. Weber, S.
802 T. Yuen, G. Harris, P. Goldstraw, A. G. Nicholson, P. A. Futreal, R. Wooster and M. R.
803 Stratton (2004). "Lung cancer: intragenic ERBB2 kinase mutations in tumours."
804 Nature **431**(7008): 525-526.
805 Tavazoie, S. F., C. Alarcon, T. Oskarsson, D. Padua, Q. Wang, P. D. Bos, W. L. Gerald and
806 J. Massague (2008). "Endogenous human microRNAs that suppress breast cancer
807 metastasis." Nature **451**(7175): 147-152.
808 Walter, A. O., R. T. Sjin, H. J. Haringsma, K. Ohashi, J. Sun, K. Lee, A. Dubrovskiy, M.
809 Labenski, Z. Zhu, Z. Wang, M. Sheets, T. St Martin, R. Karp, D. van Kalken, P. Chaturvedi,
810 D. Niu, M. Nacht, R. C. Petter, W. Westlin, K. Lin, S. Jaw-Tsai, M. Raponi, T. Van Dyke, J.
811 Etter, Z. Weaver, W. Pao, J. Singh, A. D. Simmons, T. C. Harding and A. Allen (2013).
812 "Discovery of a mutant-selective covalent inhibitor of EGFR that overcomes T790M-
813 mediated resistance in NSCLC." Cancer Discov **3**(12): 1404-1415.
814 Wu, Q., X. Hou, J. Xia, X. Qian, L. Miele, F. H. Sarkar and Z. Wang (2013). "Emerging
815 roles of PDGF-D in EMT progression during tumorigenesis." Cancer Treat Rev **39**(6):
816 640-646.
817 Wu, X., X. Liu, S. Koul, C. Y. Lee, Z. Zhang and B. Halmos (2014). "AXL kinase as a novel
818 target for cancer therapy." Oncotarget **5**(20): 9546-9563.
819 Yang, P., Q. J. Li, Y. Feng, Y. Zhang, G. J. Markowitz, S. Ning, Y. Deng, J. Zhao, S. Jiang, Y.
820 Yuan, H. Y. Wang, S. Q. Cheng, D. Xie and X. F. Wang (2012). "TGF-beta-miR-34a-CCL22
821 signaling-induced Treg cell recruitment promotes venous metastases of HBV-positive
822 hepatocellular carcinoma." Cancer Cell **22**(3): 291-303.
823 Yao, Z., S. Fenoglio, D. C. Gao, M. Camiolo, B. Stiles, T. Lindsted, M. Schlederer, C. Johns,
824 N. Altorki, V. Mittal, L. Kenner and R. Sordella (2010). "TGF-beta IL-6 axis mediates
825 selective and adaptive mechanisms of resistance to molecular targeted therapy in
826 lung cancer." Proc Natl Acad Sci U S A **107**(35): 15535-15540.
827 Zhang, L., G. Huang, X. Li, Y. Zhang, Y. Jiang, J. Shen, J. Liu, Q. Wang, J. Zhu, X. Feng, J.
828 Dong and C. Qian (2013). "Hypoxia induces epithelial-mesenchymal transition via

829 activation of SNAI1 by hypoxia-inducible factor -1alpha in hepatocellular carcinoma."
830 BMC Cancer **13**: 108.
831 Zhang, Y. X., P. G. Knyazev, Y. V. Cheburkin, K. Sharma, Y. P. Knyazev, L. Orfi, I.
832 Szabadkai, H. Daub, G. Keri and A. Ullrich (2008). "AXL is a potential target for
833 therapeutic intervention in breast cancer progression." Cancer Res **68**(6): 1905-
834 1915.
835 Zhang, Z., J. C. Lee, L. Lin, V. Olivas, V. Au, T. LaFramboise, M. Abdel-Rahman, X. Wang,
836 A. D. Levine, J. K. Rho, Y. J. Choi, C. M. Choi, S. W. Kim, S. J. Jang, Y. S. Park, W. S. Kim, D.
837 H. Lee, J. S. Lee, V. A. Miller, M. Arcila, M. Ladanyi, P. Moonsamy, C. Sawyers, T. J.
838 Boggon, P. C. Ma, C. Costa, M. Taron, R. Rosell, B. Halmos and T. G. Bivona (2012).
839 "Activation of the AXL kinase causes resistance to EGFR-targeted therapy in lung
840 cancer." Nat Genet **44**(8): 852-860.
841

842

FIGURE LEGENDS

Figure 1: AXL-positive cells are pre-existing in cell lines and tumors.

A) Immunoblot analysis of AXL in AXL-positive cells (H1650-M3 and PC14) and AXL –ve cells (H1650 and PC9). α-Tubulin is used as a loading control. **B)** Flow cytometry based analysis of surface expression of AXL in the AXL-positive cells lines (H1650-M3 and PC14) and AXL –ve cells (H1650 and PC9). Monoclonal antibody against N-terminal of AXL was used for the FACS analysis. Isotype control was used for identifying AXL-negative population. **C)** The chart represents the percentage of AXL-positive cells present in Erlotinib resistant and Erlotinib naïve cell lines. Erlotinib resistant cell lines are indicated in red, Erlotinib naïve EGFR mutant cell lines are indicated in blue, and Erlotinib naïve EGFR WT cell lines are indicated in green. Each bar represents mean ± SD of 3 replicates from two independent experiments. **D)** The chart represents relative AXL mRNA expression in the indicated cell lines or cells sorted on the basis of surface expression of AXL. Expression in AXL-positive cells was calculated relative to its expression in AXL-negative control cells. mRNA expression was quantified by SYBR-green-based RT-qPCR. Each bar represents mean ± SD of 3 replicates from two independent experiments. (p-value *** < 0.0005, **** < 0.00005, unpaired t-test). **E)** The chart represents relative Gas6 mRNA expression in the indicated cell lines or cells sorted based on surface expression of AXL. Expression in AXL-positive cells was calculated relative to its expression in AXL-negative control cells. mRNA expression was quantified by SYBR-green-based RT-qPCR. Each bar represents mean ± SD of 3 replicates from two independent experiments. (p-value *< 0.05, ** < 0.005, unpaired t-test). **F)** On the left panel**,** immunoblot analysis of AXL, GAS6, p120 RASGAP (loading control), p-AKT and AKT in AXL –ve (PC9) and AXL-positive (PC14) cells. On the right, cell extracts were immunoprecipitated with anti-AXL antibody and immunoblotted with phospho-tyrosine and AXL antibodies. Antibody heavy chain is shown as a loading control for the immunoprecipitation. **G)** The chart represents percentage of AXL-positive cells in six NSCLC patient tumors. Tumor-derived single cell suspension was stained with antibodies against CD45, CD31, EpCAM, and AXL. CD45-; CD31-; EpCAM+ cells were then FACS sorted for the AXL-positive populations. Each bar represents mean ± SD of three technical replicates. 20,000 cells were analyzed by FACS for each replicate of each sample. Schematic of the FACS sorting is presented in Figure 1-figure supplement 2. **H)** Expression of *AXL and GAS6* genes in FACS-sorted AXL–negative (Blue) and AXL-positive (Red) cells from five human primary NSCLC tumors. mRNA expression was quantified by Cells to CT one step SYBR-green-based RT-qPCR. Expression of an indicated

mRNA in the AXL-positive cells was calculated relative to its expression in AXL-negative cells from the respective tumor. Each dot represents mean ± SD of three replicates.

Figure 1-figure supplement 1: FACS sorting algorithm utilized to sort human tumors

Single cell suspensions generated from resected primary NSCLC were stained with antibodies against CD45, CD31, EpCAM and AXL. CD45-; CD31-; EpCAM+ cells were then FACS sorted according to the immune types AXL –ve and AXL-positive (shown in red). Isotype controls were used to determine negative populations for each antibody staining.

Figure 2: Pre-existing AXL-positive cells have characteristics of Erlotinib resistant cells.

A) The chart represents the number of viable cells in PC9, PC14 and AXL-positive cells sorted from PC9 upon treatment with indicated doses of Erlotinib. Values are normalized relative to vehicle treated cell (control). Cells were grown for 120 hours in the presence of drug; the number of cells were estimated upon staining with the crystal violet, de-staining in 100 µl of 10% acetic acid and reading absorbance at 590 nm. Diamonds and black bars represent single point measurements and the mean respectively (n=6); (p-value *< 0.05, ** < 0.005, *** < 0.0005, unpaired t-test). **B)** AXL-positive cells are characterized by mesenchymal features such as increase in stress fibers. AXL–negative and AXL-positive cells sorted from PC9 were stained F-actin with Phalloidin (green). DAPI (blue) was used as a counter-stain. **C)** The charts represent relative expression of the indicated mesenchymal signature genes in H1650, H1650-M3 and cells sorted on the basis of surface expression of AXL from H1650 and PC9. Expression of an indicated mRNA in the AXL-positive cells was calculated relative to its expression in AXL-negative control cells mRNA expression was quantified by SYBR-green-based RT-qPCR. Each bar represents mean ± SD of 3 replicates from two independent experiments. (p-value *< 0.05, ** < 0.005, *** < 0.0005, **** < 0.00005, unpaired t-test). **D)** Expression of mesenchymal signature genes *VIM*, *TWIST* and *ZEB1* in FACS-sorted AXL-negative (Blue) and AXL-positive (Red) cells from five human primary NSCLC tumors. mRNA expression was quantified by Cells to CT one step SYBR-green-based RT-qPCR. Expression of an indicated mRNA in the AXL-positive cells was calculated relative to its expression in AXL-negative cells from the respective tumor. Each dot represents mean ± SD of three replicates.

Figure 2-figure supplement 1: Pre-existing AXL-positive cells have characteristics of Erlotinib resistant cells. **A)** and **B)** Pre-existent AXL-positive cells preferentially persist during drug treatment. The charts represent the percentage of viable cells in the indicated populations upon

910 treatment with Erlotinib (0,5 μM) (A) and Gefitinib (1μM) (B). AXL-positive cells were sorted
911 from PC9, and stably infected with lentivirus expressing Td-Tomato. Then AXL-negative and Td-
912 Tom AXL-positive cells were mixed in the mentioned ratio and treated with the EGFR TKIs. Please
913 see the methods section for further details. **C)** AXL-negative and AXL-positive FACS-sorted cells
914 from H1650; parental H1650 and erlotinib selected AXL-positive H1650-M3 cells; PC9 and
915 erlotinib selected AXL-positive PC14 cells were stained with Phalloidin (green) to highlight stress
916 fibers. DAPI (blue) was used as a counter-stain. **D)** The chart represents relative expression of the
917 indicated mesenchymal signature genes in cells sorted based on surface expression of AXL from
918 HCC827. Expression of an indicated mRNA in the AXL-positive cells was calculated relative to
919 its expression in AXL-negative control cells mRNA expression was quantified by SYBR-green-
920 based RT-qPCR. Each bar represents mean ± SD of 3 replicates from two independent experiments.
921 (p-value *< 0.05, ** < 0.005, *** < 0.0005, **** < 0.00005, unpaired t-test). **E)** Pharmacological
922 inhibition of AXL leads to significant mesenchymal to epithelial transition specifically in AXL-
923 positive cells. The charts represent expression of E-cadherin and Vimentin in AXL-positive
924 (H1650-M3) cells and AXL-negative (H1650) cells upon treating with the AXL inhibitor BMS-
925 777607 at the indicated concentration. mRNA expression was quantified by SYBR-green-based
926 RT-qPCR. Each bar represents mean ± SD of 3 replicates from two independent experiments. (p-
927 value *< 0.05, unpaired t-test). ns = non-significant.
928
929 **Figure 2-figure supplement 2: AXL-positive cells are a unique cell population.**
930 **A)** The table summarizes the molecular characteristics of the indicated panel of NSCLC cell lines.
931 **B)** The cells were stained with antibodies against E-cadherin (RED) and Vimentin (Green) to verify
932 their epithelial or mesenchymal cell state. DAPI (blue) was used as a counter-stain. **C)** Flow
933 cytometry based analysis of surface expression of AXL in the panel of NSCLC cell lines to
934 determine the percentage of pre-existing AXL-positive cells. Monoclonal antibody against N-
935 terminal of AXL was used for the FACS analysis. Isotype control was used for identifying AXL-
936 negative population. Isotype control was used for identifying AXL-negative population (not
937 shown).
938
939 **Figure 3: AXL-positive cells are generated stochastically.**
940 **A)** If AXL-positive cells (red) were generated as a consequence of genetic mutations, single-cell
941 derived clones will have different percentages of AXL-positive cells. **B)** On the other hand, if AXL-
942 positive cells were generated stochastically, then an equal percentage of AXL-positive cells will be
943 present in both parental and single cell derived isogenic clones. **C)** and **D)** The charts represent the

944 percentage of AXL-positive cells in the parental and single cell derived clonal populations in
945 H1650 and HCC827 respectively. Cells were stained for surface expression of AXL, followed by
946 flow cytometry analysis. Each bar represents mean ± SD of three technical replicates from two
947 independent experiments. 20,000 cells were analyzed by FACS for each replicate of each sample.
948 **E)** AXL negative (Blue) and AXL-positive (Red) cells were sorted from H1650 cell line and were
949 grown for 18 weeks. The percentage of AXL-positive cells emerging in each population was
950 measured weekly, and represented as dots in the chart. The red dotted line represents the percentage
951 of AXL-positive cells that were present in the total H1650 parent cell line. **F)** AXL –ve (Blue) and
952 AXL-positive (Red) cells were sorted from single cell derived clonal cell line from H1650 (H1650
953 Clone 2), and were grown for 18 weeks. The percentage of AXL-positive cells emerging in each
954 population was measured weekly, and represented as dots in the chart. The red dotted line
955 represents the percentage of AXL-positive cells that were present in the total H1650 clone 2 cell
956 line.
957
958 **Figure 3-figure supplement 1: Parental cell lines and single cell derived clonal cell lines**
959 **(H1650 and HCC827) are highly similar from a molecular standpoint.** The charts represent the
960 mRNA expression of AXL and key mesenchymal genes in the parental and single cell derived
961 clonal cell lines (H1650 and HCC827).
962
963 **Figure 4: miRNA profiling reveals a distinct signature that characterize the AXL-positive**
964 **cell-state.**
965 **A)** and **B)** The bubble charts show miRNAs that were >2 fold upregulated or >2 fold downregulated
966 in AXL-positive (H1650-M3) cells relative to the parental AXL-negative (H1650) cells. Small
967 RNA libraries were generated from each cell line and sequenced using an Illumina platform. The
968 size of the bubble represents the abundance of the miRNA. **C)** Heat map depicts patterns of miRNA
969 expression in AXL-negative (H1650) and AXL-positive (H1650-M3) cells, validated by
970 quantitative stem-loop RT-PCR. Columns indicate relative expression changes compared to U6
971 snRNA. Each square represents the average of 3 independent measurements. p-value ≤0.0001,
972 unpaired t-test. **D)** miR-335 targets are increasingly expressed in AXL-positive cells. The heat map
973 on the left shows changes in mRNA expression of miR-335 targets in AXL-negative (H1650) and
974 AXL-positive (H1650-M3) cells. Each column represents changes in mRNAs expression relative
975 to Actin. Each square represents the average of 3 independent measurements. p-value ≤0.0001,
976 unpaired t-test. **E)** The chart represents expression of miR-335 normalized to SNORA66 in the
977 indicated cell lines. miRNA expression was quantified by ExiLENT SYBR-green-based RT-qPCR.

Each bar represents mean ± SD of 3 replicates from two independent experiments. (p-value *< 0.05, unpaired t-test). **F)** The chart represents expression of miR-335 normalized to SNORA66 in AXL –ve (Blue) and AXL-positive (Red) cells sorted from H1650 and HCC827 cell lines. miRNA expression was quantified by ExiLENT SYBR-green-based RT-qPCR. Each bar represents mean ± SD of 3 replicates from two independent experiments. (p-value *< 0.05, unpaired t-test). **G)** The chart represents expression of miR-335 normalized to SNORA66 in AXL –ve (Blue) and AXL-positive (Red) cells sorted from four human primary NSCLC tumors. miRNA expression was quantified by ExiLENT SYBR-green-based RT-qPCR. Each dot represents mean ± SD of 3 replicates. **H)** The chart represents expression of the indicated miRNAs normalized to SNORA66 in AXL –ve H1650 cells treated with Vehicle (Blue) or TGF-beta (Red). The data are presented as relative to vehicle treated control. miRNA expression was quantified by ExiLENT SYBR-green-based RT-qPCR. Each bar represents mean ± SD of 3 replicates from two independent experiments. (p-value *< 0.05, **< 0.005, paired t-test). ns= non-significant. **I)** The chart represents expression of the indicated miRNAs normalized to SNORA66 in AXL-positive H1650-M3 cells treated with Vehicle (Red) or TGFbRI inhibitor LY2157299, Selleckchem (Red). The data are presented as relative to vehicle treated control. miRNA expression was quantified by ExiLENT SYBR-green-based RT-qPCR. Each bar represents mean ± SD of 3 replicates from two independent experiments. (p-value *< 0.05, **< 0.005, ***< 0.005 paired t-test). ns= non-significant. **H)** The chart represents expression of the indicated miRNAs normalized to SNORA66 in AXL –ve H1650 cells treated with Scramble LNA (Blue) or miR-335 antagomir (Red). The data are presented as relative to scramble treated control. miRNA expression was quantified by ExiLENT SYBR-green-based RT-qPCR. Each bar represents mean ± SD of 3 replicates from two independent experiments. (p-value *< 0.05, **< 0.005, paired t-test).

Figure 4-figure supplement 1: Inhibiting miR-335 expression results in re-expression of miR-335 targets. A) The Histogram shows miR-335 levels in H1650 cells upon 5 days of treatment with three independent miR-335 antagomirs (see material section for information) in H1650 cells. Levels of miR-335 expression are relative to SNORA66. Each bar represents mean ± SD of 3 replicates from two independent experiments. (p-value ** < 0.005, *** < 0.0005 unpaired t-test). **B)** Expression of miR-335 targets in H1650 cells upon treatment with miR-335 antagomirs relative to control. Each bar represents mean ± SD of 3 replicates from two independent experiments. (p-value * < 0.05, ** < 0.005, ** < 0.0005, *** <0.00005, # <0.000005 unpaired t-test). **C)** The chart represents the relative expression of TGF-β1 and 2 in AXL-negative H1650 cells treated with scramble LNA (Blue) or miR-335 antagomir (Red). The data are presented as relative to scramble

treated control. mRNA expression was quantified by SYBR-green-based RT-qPCR. Each bar represents mean ± SD of 3 replicates from two independent experiments. (p-value *< 0.05, paired t-test).

Figure 5: miR-335 regulates AXL-positive cell-state transition.

A) The chart on left represents the knockdown efficiency of miR-335 antagomir in H1650 and PC9 cells. mRNA expression was quantified by SYBR-green-based RT-qPCR and normalized to GAPDH. Each bar represents mean ± SD of 3 replicates from two independent experiments. (p-value * < 0.05, unpaired t-test). **B)** The chart represents the percentage of AXL-positive cells present in H1650 and PC9 cells upon treatment with miR-335 antagomir relative to scramble treated control. Cells stained with antibody against N-terminal of AXL were used for FACS analysis. Each bar represents mean ± SD of three technical replicates. 20,000 cells were analyzed by FACS for each replicate of each sample. (p-value * < 0.05, unpaired t-test). See Figure 5-figure supplement 1A for representative FACS profiles. **C)** Representative images of H1650 and PC9 cells stained with Phalloidin (green) and DAPI (blue) as counterstain. Cells were treated for 5 days with control antagomir or miR-335 antagomir. **D)** Fold change in genes that characterize the AXL-positive cell-state upon inhibition of miR-335 in AXL –ve cell lines H1650 and PC9. mRNA expression was quantified by SYBR-green-based RT-qPCR and normalized to actin. Each bar represents mean ± SD of 3 replicates from two independent experiments. (p-value * < 0.05, ** < 0.005, ***< 0.0005 unpaired t-test). **E)** The charts represent the number of viable cells in H1650 and **F)** PC9 cells upon transfection with miR-335 antagomir and treatment with indicated doses of Erlotinib. Values are normalized relative to vehicle treated cell (control). Cells were grown for 120 hours in the presence of drug; the number of cells was estimated upon staining with the crystal violet, de-staining in 100 µl of 10% acetic acid and reading absorbance at 590 nm. Diamonds and black bars represent single point measurements and the mean respectively (n=8); (p-value ** < 0.005, unpaired t-test). ns = non-significant.

Figure 5-figure supplement 1: Inhibiting miR-335 expression results in molecular and phenotypic changes characteristic of the AXL-positive cell-state.

A) Flow cytometry based analysis of surface expression of AXL in PC9 and H1650 cells upon inhibition of miR-335 with miR-335 antagomir, to determine the change in percentage of AXL-positive cells. Monoclonal antibody against N-terminal of AXL was used for the FACS analysis. Isotype control was used for identifying AXL-negative population. Isotype control was used for identifying AXL-negative population (not shown).

Figure 5-figure supplement 2: CRISPR-CAS9 mediated gene editing to reduce miR-335 expression results in molecular and phenotypic changes characteristic of the AXL-positive cell-state.

A) The chart represents the knock down efficiency of the indicated small guide RNAs (sg. RNA) targeting the miR-335 sequence, compared to cells receiving sg.Renilla (control). mRNA expression was quantified by SYBR-green-based RT-qPCR. Each bar represents mean ± SD of 3 replicates from two independent experiments. (p-value **< 0.005, paired t-test). **B)** Flow cytometry based analysis of surface expression of AXL in H1650 cells upon editing the miR-335 sequence with three different guide RNAs, to determine the change in percentage of AXL-positive cells. sg.RNA against Renilla is used as a control. Monoclonal antibody against N-terminal of AXL was used for the FACS analysis. Isotype control was used for identifying AXL-negative population. Isotype control was used for identifying AXL-negative population (not shown). **C)** The chart represents the fold change in the mRNA expression of the indicated genes in H1650 cells containing sg. RNAs targeting the miR-335 sequence or Renilla (control), and presented relative to Renilla control. mRNA expression was quantified by SYBR-green-based RT-qPCR. Each bar represents mean ± SD of 3 replicates from two independent experiments. (p-value *< 0.05, **< 0.005, paired t-test).

Figure 6: Methylation of MEST isoform 2 promoter modulates miR-335 expression in AXL-positive cells.

A) Schematic of MEST locus organization; the methylation analysis by bisulfite sequencing of MEST CpG island 1 and 2 in AXL –ve (H1650) and AXL-positive (H1650-M3) cells lines are shown below. **B)** Semi-quantitative RT-PCR analysis of methylation status of CpG island 1 in H1650 and H1650-M3. U: Un-methylation specific primer; M: Methylation specific primer. See Figure 6-figure supplement 1A for relative amount of methylation of MEST CpG island 1 in the Erlotinib naïve and reistant cell lines quantified via methylation specific SYBR-green-based RT-qPCR (MSP). **C)** The chart represents relative amount of methylation of MEST CpG island 1 in AXL –ve (Blue) and AXL-positive (Red) cells sorted from H1650 and PC9 cell lines. Amount of methylation of DNA was quantified via methylation specific SYBR-green-based RT-qPCR (MSP). Each bar represents mean ± SD of 3 replicates from two independent experiments. (p-value *< 0.05, unpaired t-test). **D)** The chart represents relative amount of methylation of MEST CpG island 1 in AXL –ve (Blue) and AXL-positive (Red) cells sorted from 4 human primary NSCLC tumors. Amount of methylation of DNA was quantified via methylation specific SYBR-green-based RT-

qPCR (MSP). Each dot represents mean ± SD of three replicates. **E-H)** Treatment of cells with 5-aza-dC is sufficient to reduce the levels of CpG island 1 methylation, increase the expression of miR-335 decrease AXL-positive cells and reduce Erlotinib resistance, respectively. **E)** The chart represents the relative amount of methylation of MEST CpG island 1 in H1650 and H1650-M3 cells treated with indicated amount of 5-aza-dC. Amount of methylation of DNA was quantified via methylation specific SYBR-green-based RT-qPCR (MSP). Each bar represents mean ± SD of 3 replicates from two independent experiments. (p-value *< 0.05, unpaired t-test). ns = non-significant. **F)** The chart represents the amount of miR-335 (relative to SNORA66) in H1650 and H1650-M3 cells upon treatment with 5-aza-dC, and normalized to vehicle treated control. miRNA expression was quantified by ExiLENT SYBR-green-based RT-qPCR. Each bar represents mean ± SD of 3 replicates from two independent experiments. (p-value *< 0.05, unpaired t-test). ns = non-significant. **G)** The chart represents percentage of AXL-positive cells in H1650-M3 upon treatment with 5-aza-dC, in presence of scramble LNA (RED solid bar) or miR-335 antagomir (dotted bar). The data is presented relative to H1650-M3 cells treated with scramble LNA at 0nM 5-aza-dC. Cells stained with antibody against N-terminal of AXL were used for FACS analysis. Each bar represents mean ± SD of three technical replicates. 20,000 cells were analyzed by FACS for each replicate of each sample. (p-value * < 0.05, ** < 0.005, *** < 0.05 unpaired t-test). ns = non-significant. See Figure 6-figure supplement 1C for the representative mRNA expression. **H)** The chart represents the relative number of Erlotinib surviving colonies in absence of presence of 5-aza-dC. Compared to the AXL –ve cells, the AXL-positive cells have significantly higher number of surviving colonies, that in presence of 5-aza-dC reduced. Each bar represents mean ± SD of 3 replicates from two independent experiments. (p-value *< 0.05, unpaired t-test). ns = non-significant.

Figure 6-figure supplement 1: A) The chart represents relative amount of methylation of MEST CpG island 1 in the H1650, H1650-M3, PC9 and PC14 cell lines. Amount of methylation of DNA was quantified via methylation specific SYBR-green-based RT-qPCR (MSP). Each bar represents mean ± SD of 3 replicates from two independent experiments. (p-value *< 0.05, unpaired t-test). **B)** The chart represents relative amount of methylation of MEST CpG island 1 in AXL –ve (Blue) and AXL-positive (Red) cells sorted from HCC827 and A549 cell lines. Amount of methylation of DNA was quantified via methylation specific SYBR-green-based RT-qPCR (MSP). Each bar represents mean ± SD of 3 replicates from two independent experiments. (p-value *< 0.05, unpaired t-test). **C)** The chart represents relative expression of AXL mRNA in H1650-M3 upon treatment with 5-aza-dC, in presence of scramble LNA (RED solid bar) or miR-335 antagomir

(dotted bar). The data is presented relative to H1650-M3 cells treated with scramble LNA at 0nM 5-aza-dC. mRNA expression was quantified by SYBR-green-based RT-qPCR. Each bar represents mean ± SD of 3 replicates from two independent experiments. (p-value * < 0.05, ** < 0.005, *** < 0.0005, unpaired t-test). ns= non-significant. **D)** The chart represents percentage of AXL-positive cells in AXL –ve cells (Blue) and AXL-positive cells (Red) sorted from H1650 upon treatment with 5-aza-dC. (p-value ** < 0.005, unpaired t-test). ns= non-significant.

Figure 7: Cancer cells can transit between an epithelial state characterized by low expression of AXL and a mesenchymal-like state with high AXL expression. AXL-positive cells have increased resistance to EGFR TKi compared to AXL-negative cells. The transition between these two states is rstricted by miR-335 whose expression is regulated epigenetically through promoter methylation. The existence of this innate stochastic/epigenetic mechanism has important therapeutic implications. Upon treatment with EGFR TKi, AXL-positive cells can survive but differently from cells that have acquired resistance through genetic mutations with time they can revert to an epithelial EGFR TKi sensitive state.

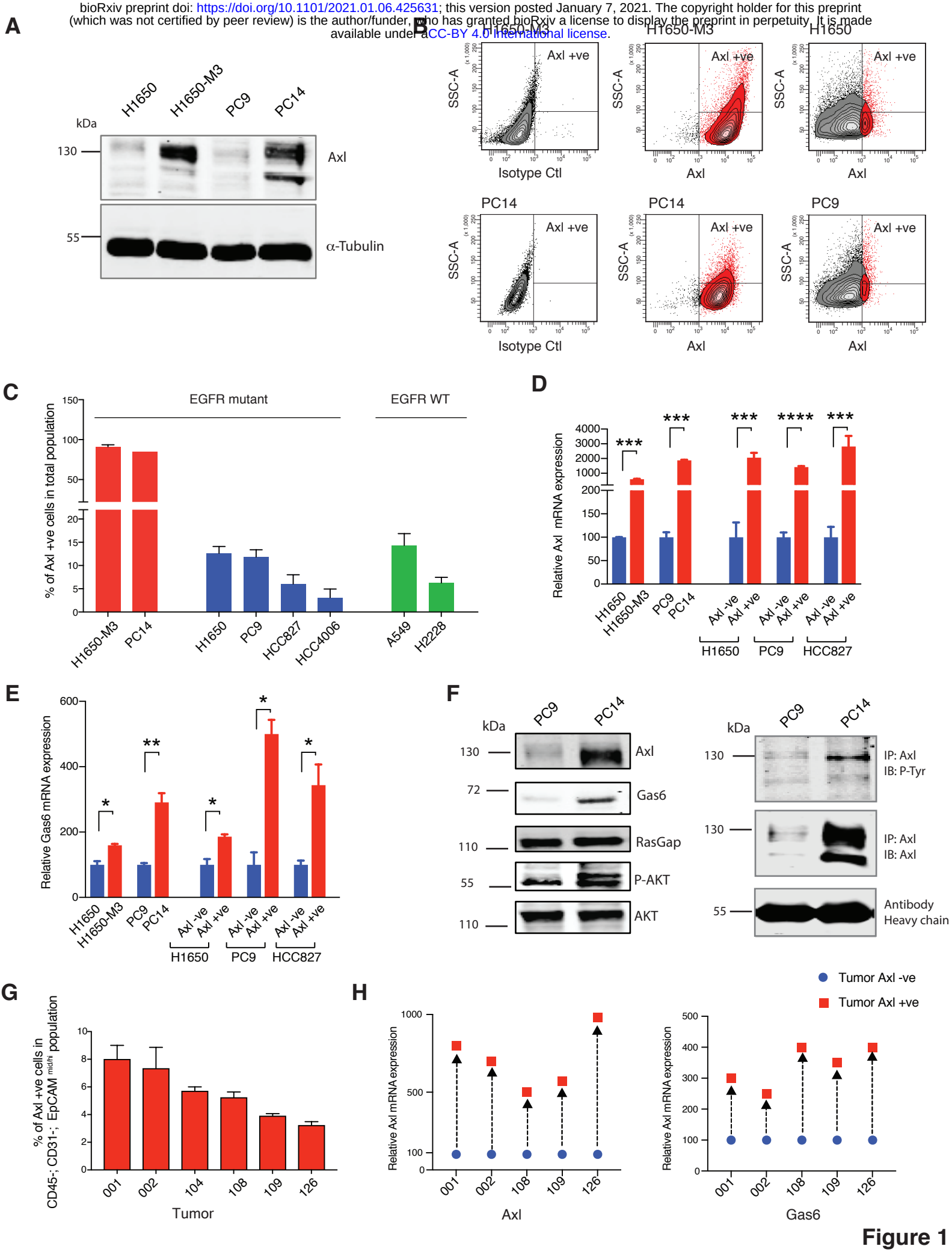

Figure 1

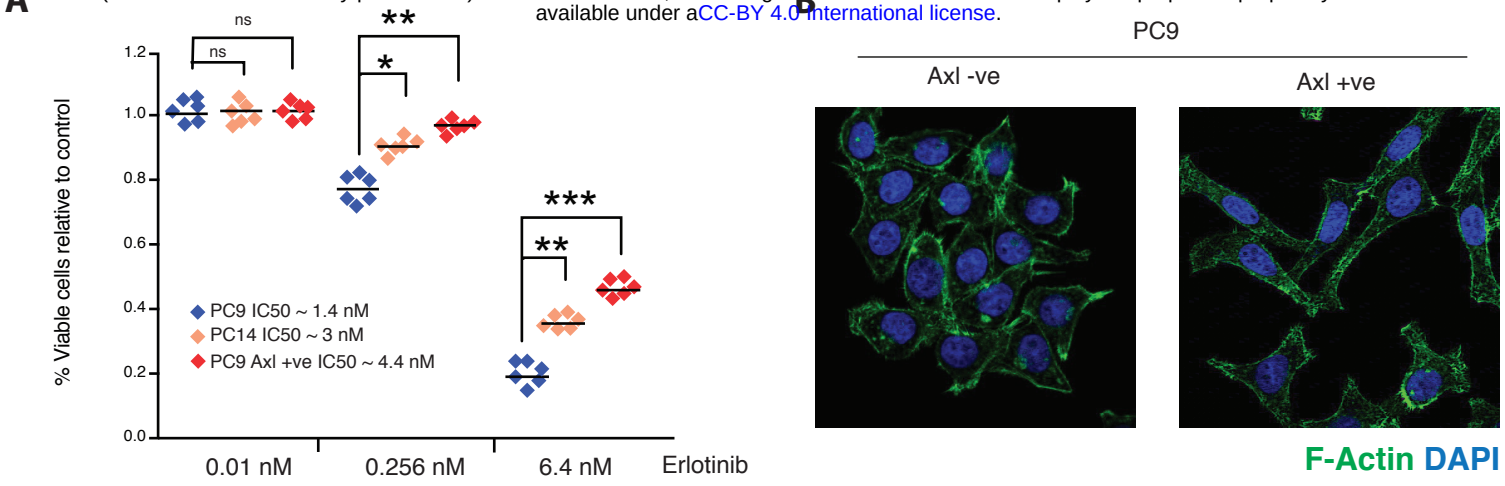

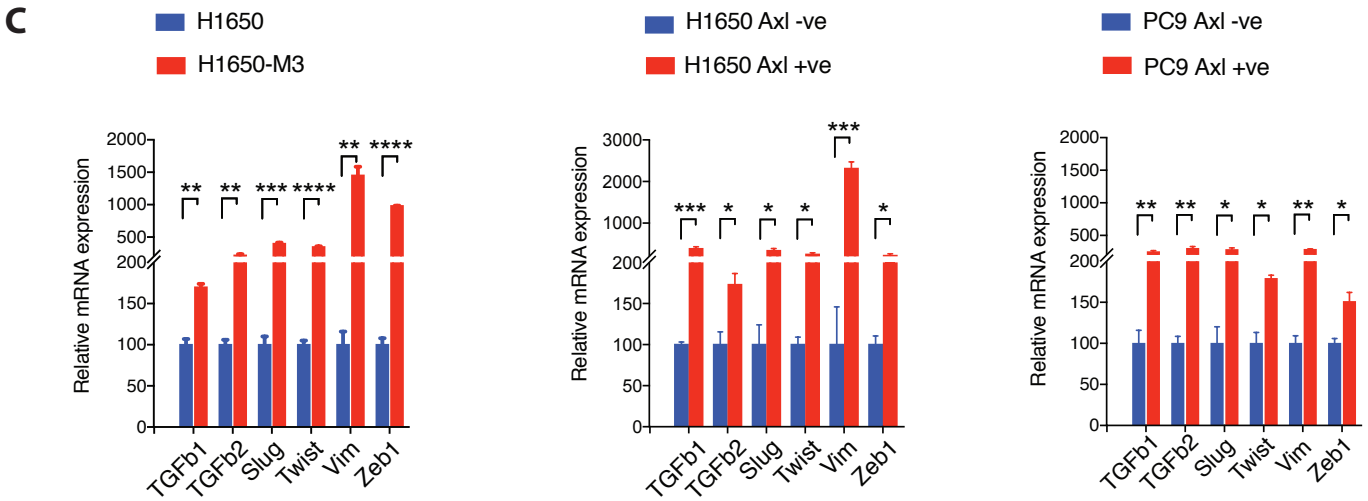

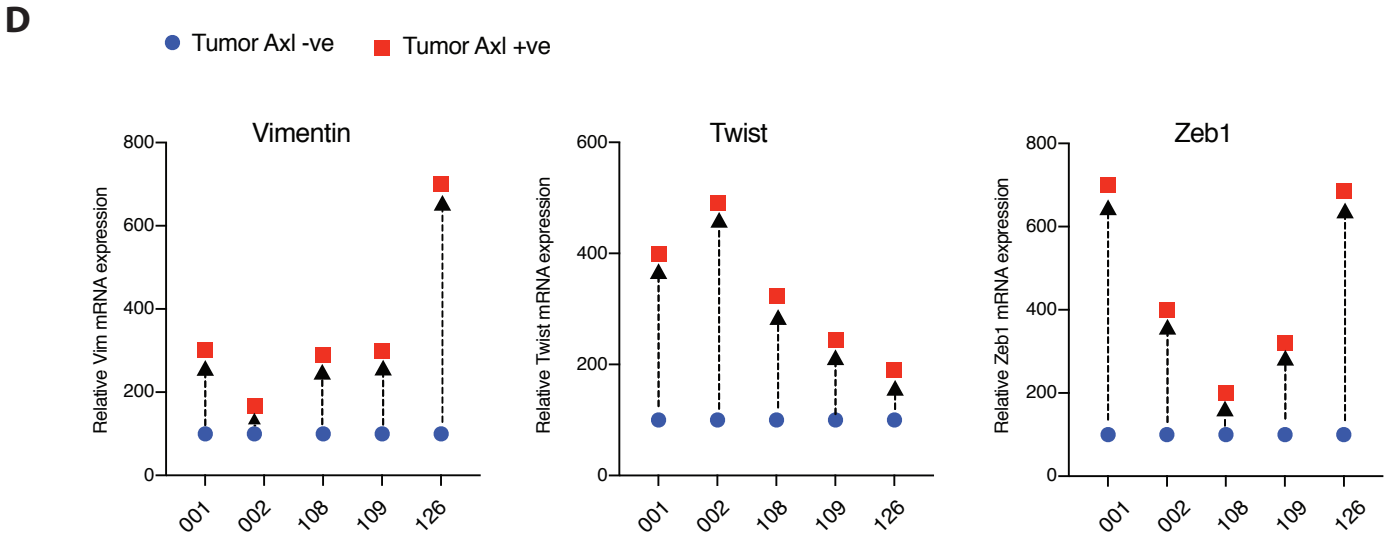

Figure 2

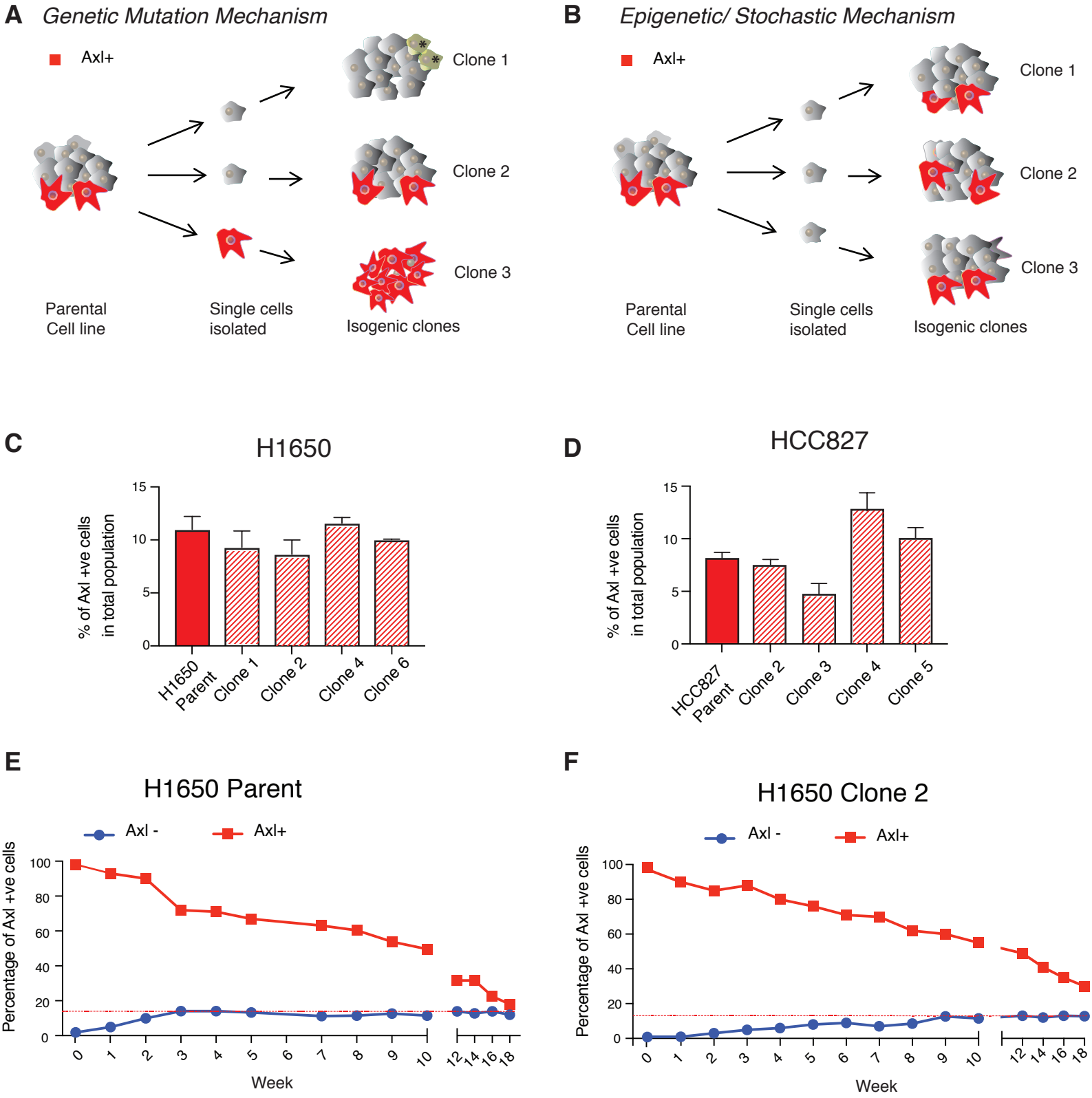
A
Genetic Mutation Mechanism
Axl+
Clone 1
Clone 2
Clone 3
Parental Cell line
Single cells isolated
Isogenic clones
B
Epigenetic/ Stochastic Mechanism
Axl+
Clone 1
Clone 2
Clone 3
Parental Cell line
Single cells isolated
Isogenic clones
C
H1650
% of Axl +ve cells in total population
15
10
5
0
H1650 Parent
Clone 1
Clone 2
Clone 4
Clone 6
D
HCC827
% of Axl +ve cells in total population
15
10
5
0
HCC827 Parent
Clone 2
Clone 3
Clone 4
Clone 5
E
H1650 Parent
Axl -
Axl+
Percentage of Axl +ve cells
100
80
60
40
20
0
0 1 2 3 4 5 6 7 8 9 10 12 14 16 18
Week
F
H1650 Clone 2
Axl -
Axl+
Percentage of Axl +ve cells
100
80
60
40
20
0
0 1 2 3 4 5 6 7 8 9 10 12 14 16 18
Week

Figure 3

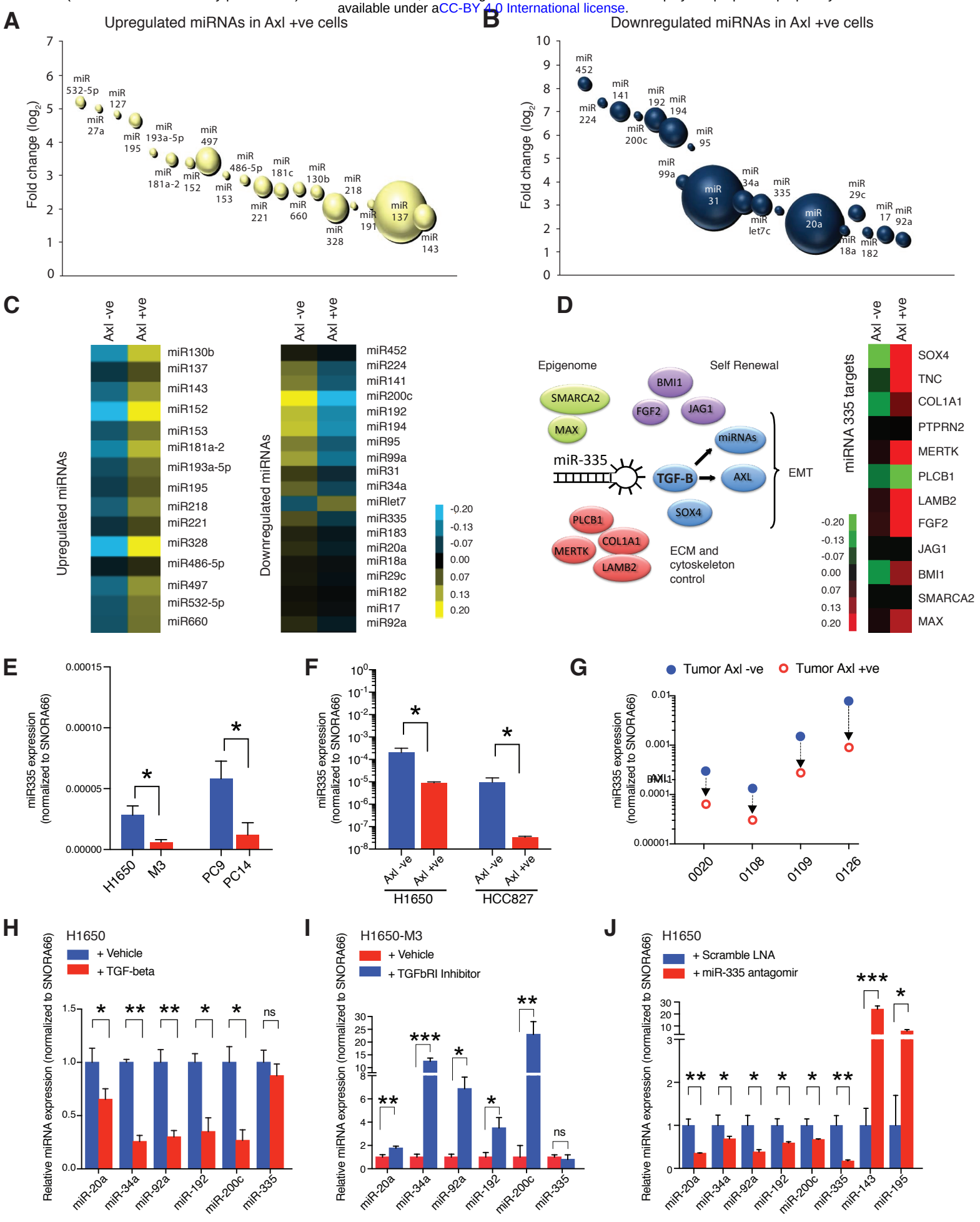

Figure 4

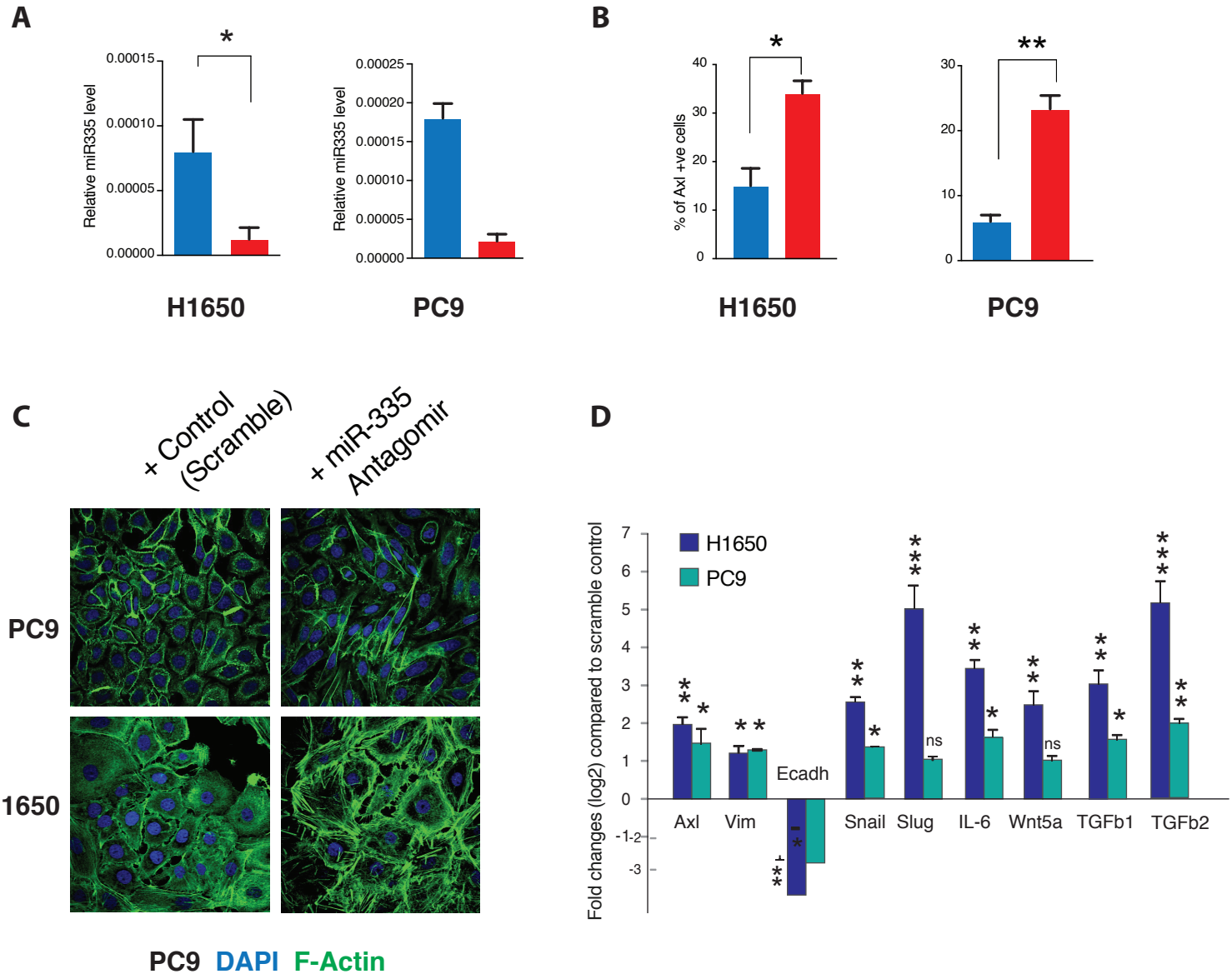

Figure 5

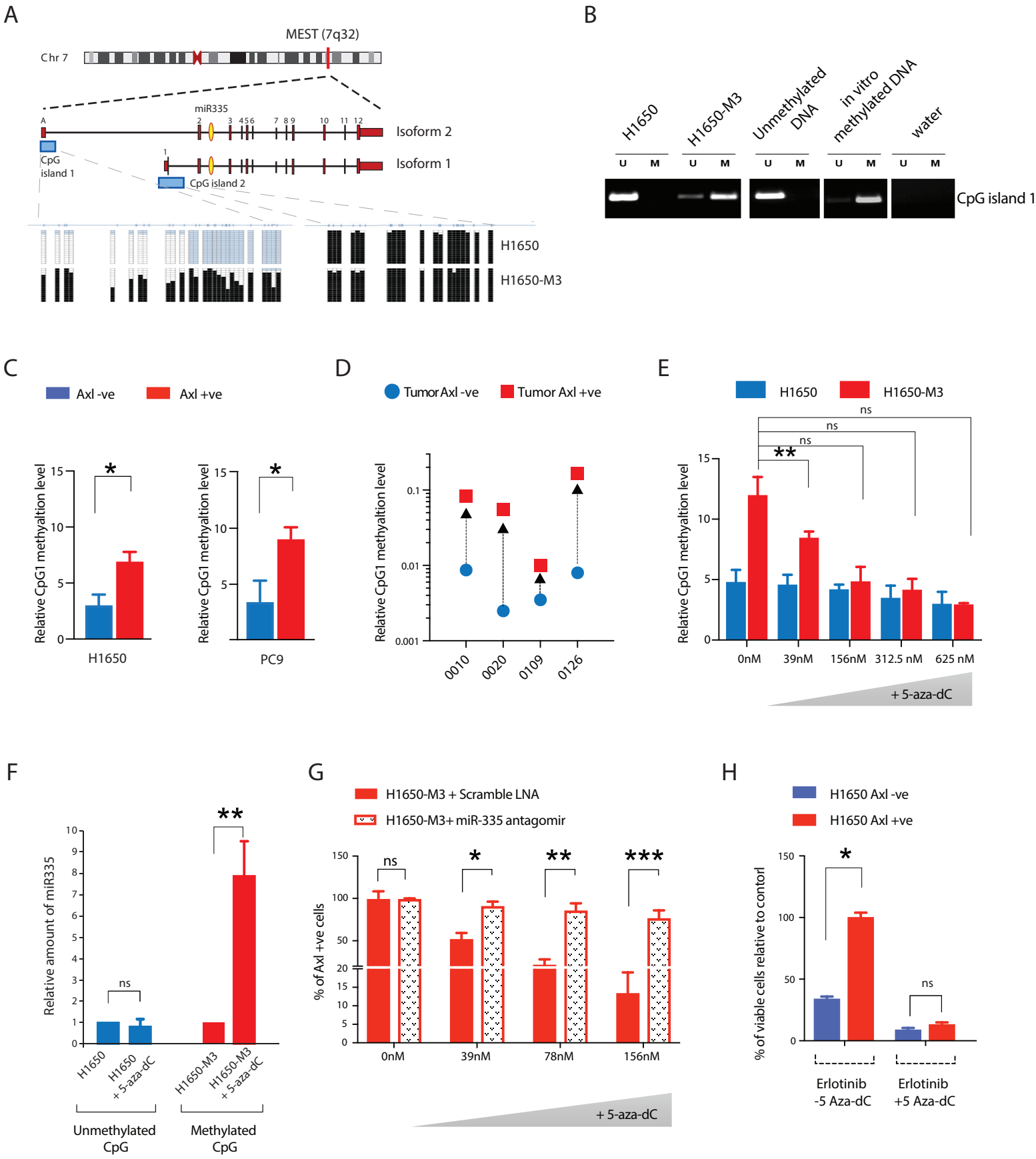
A
MEST (7q32)
Chr 7
miR335
Isoform 2
Isoform 1
CpG island 1
CpG island 2
H1650
H1650-M3
B
H1650
H1650-M3
Unmethylated DNA
in vitro methylated DNA
water
U
M
CpG island 1
C
Axl -ve
Axl +ve
Relative CpG1 methyaltion level
H1650
PC9
D
Tumor Axl -ve
Tumor Axl +ve
0010
0020
0109
0126
E
H1650
H1650-M3
ns
**
0nM
39nM
156nM
312.5 nM
625 nM
+ 5-aza-dC
F
Relative amount of miR335
ns
H1650
H1650 + 5-aza-dC
H1650-M3
H1650-M3 + 5-aza-dC
Unmethylated CpG
Methylated CpG
G
H1650-M3 + Scramble LNA
H1650-M3+ miR-335 antagomir
% of Axl +ve cells
0nM
39nM
78nM
156nM
+ 5-aza-dC
H
H1650 Axl -ve
H1650 Axl +ve
% of viable cells relative to contorl
Erlotinib -5 Aza-dC
Erlotinib +5 Aza-dC

Figure 6

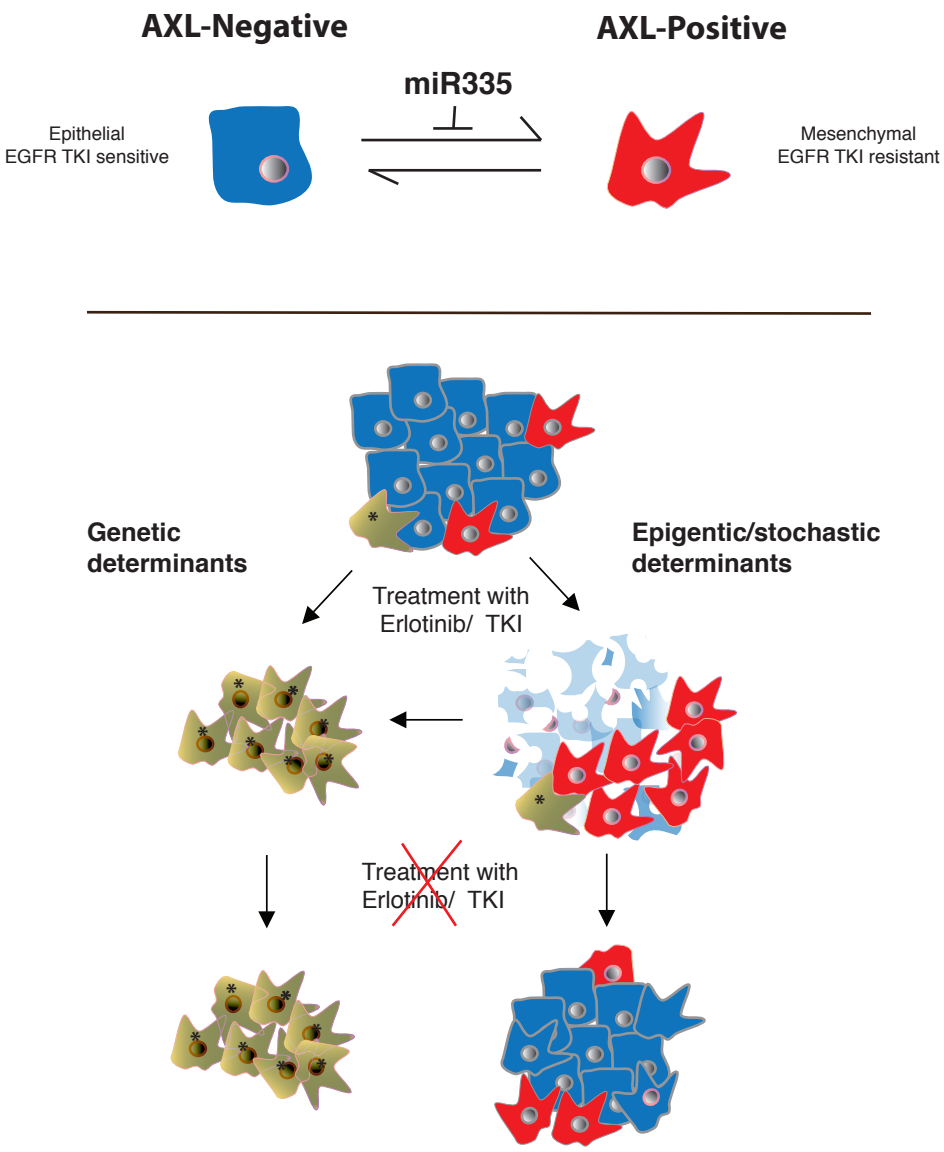

Figure 7

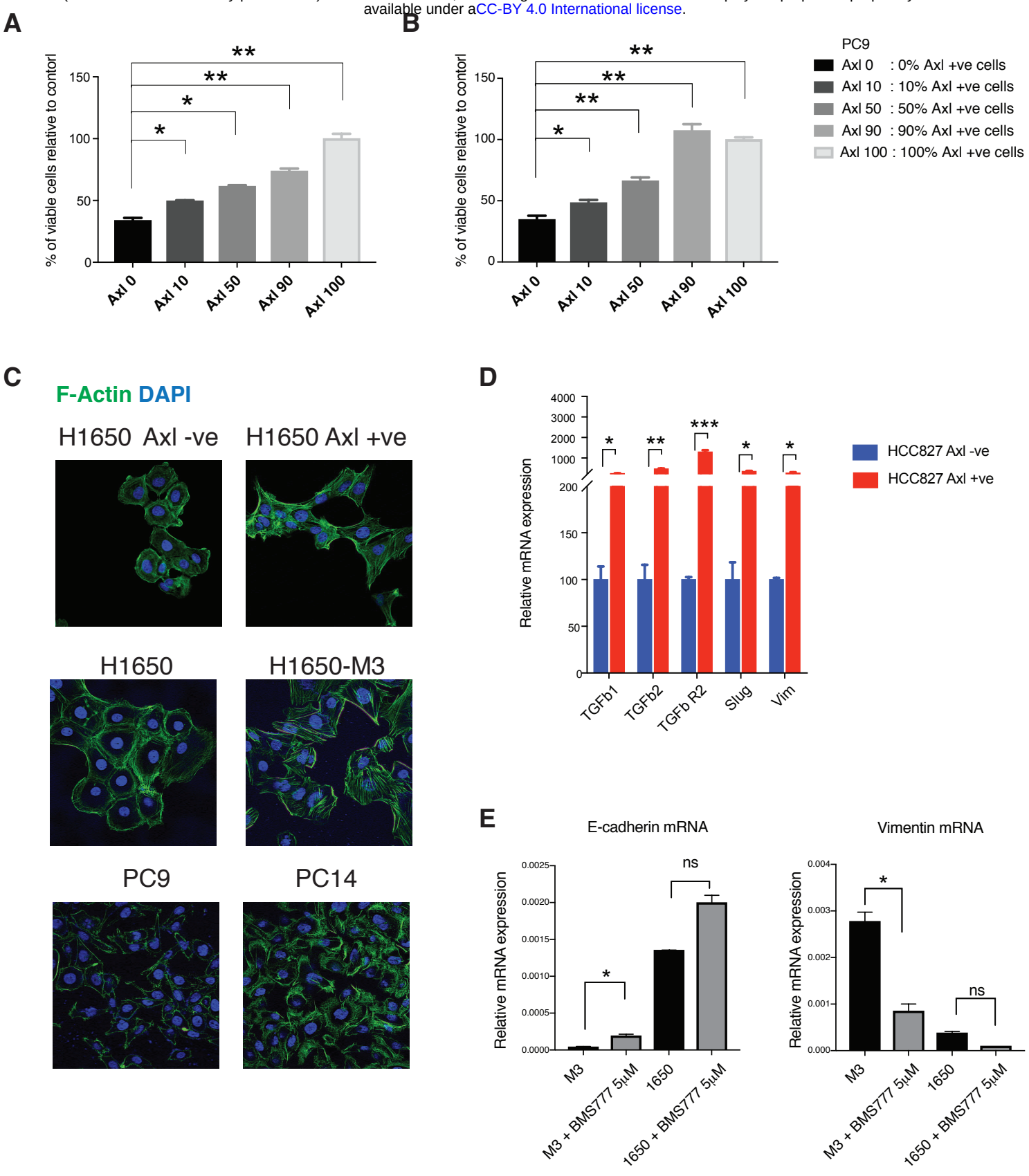

Figure 2-figure supplement 1

A

Cell Line	EGFR activating Mutations	Another mutation/ driver oncogene	Phenotype
H1650	delE746-A750		Epithelial
A549	WT	KRAS G12S	Epithelial
PC9	delE746-A750		Intermediate
H23	WT		Mesenchymal
H1650-M3	delE746-A750		Mesenchymal
H1703	WT	PDGFR overexpression	Mesenchymal
H1975	L858R/ T790M		Mesenchymal

B

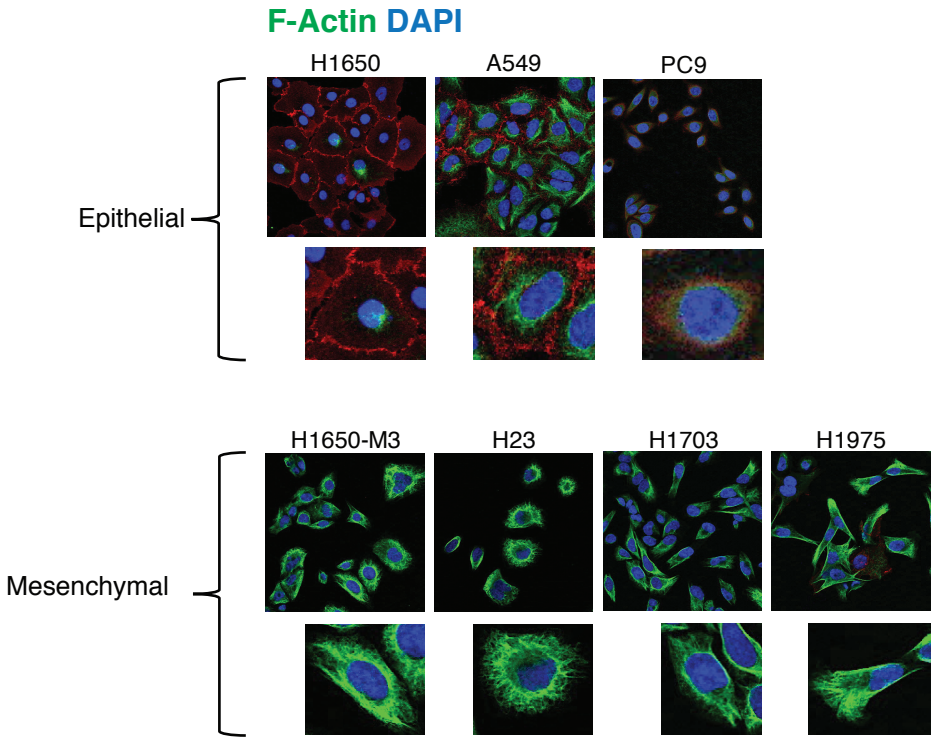

C

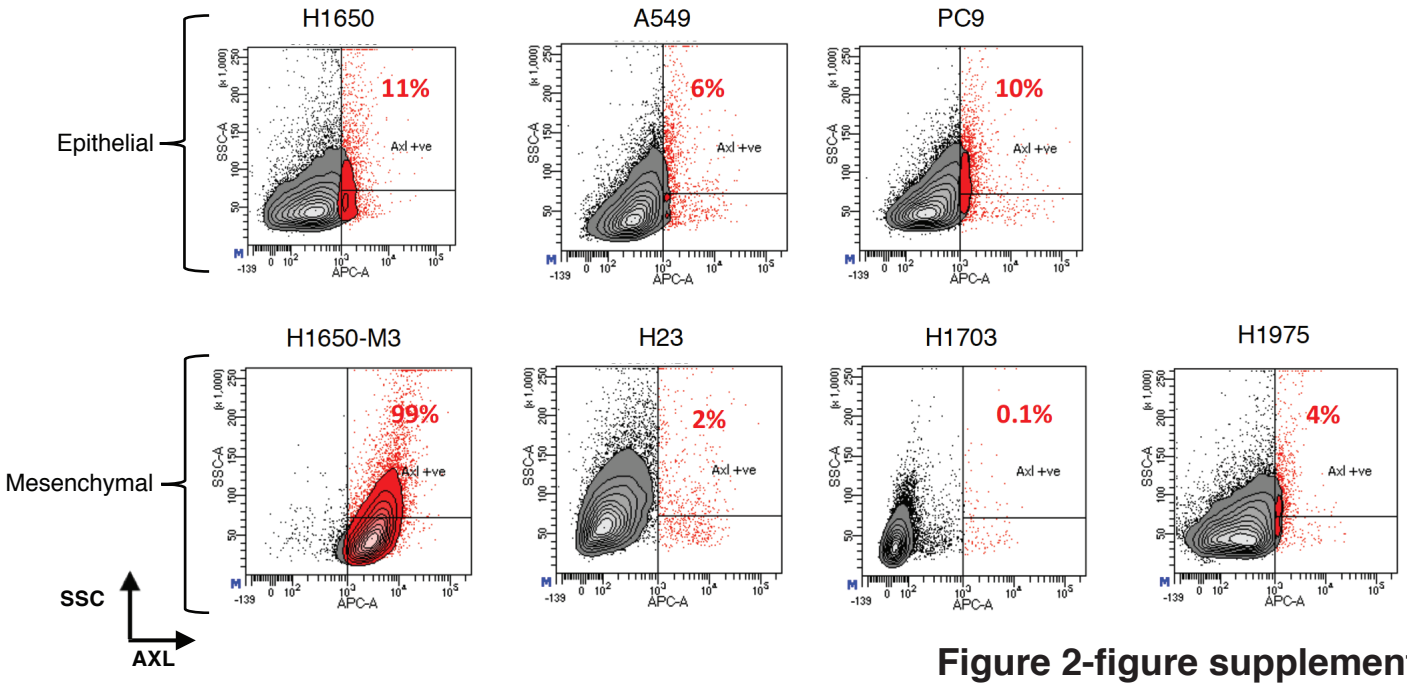

Figure 2-figure supplement 2

A

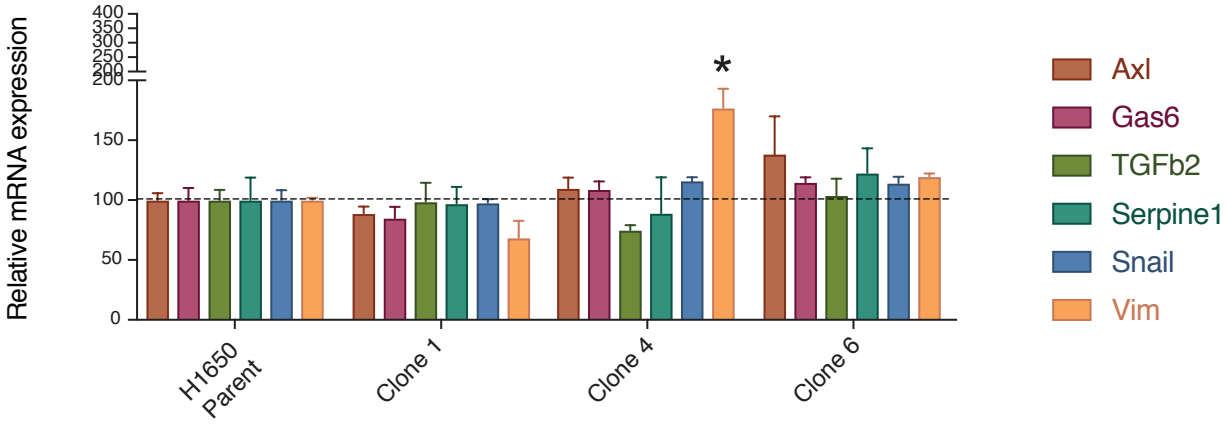

B

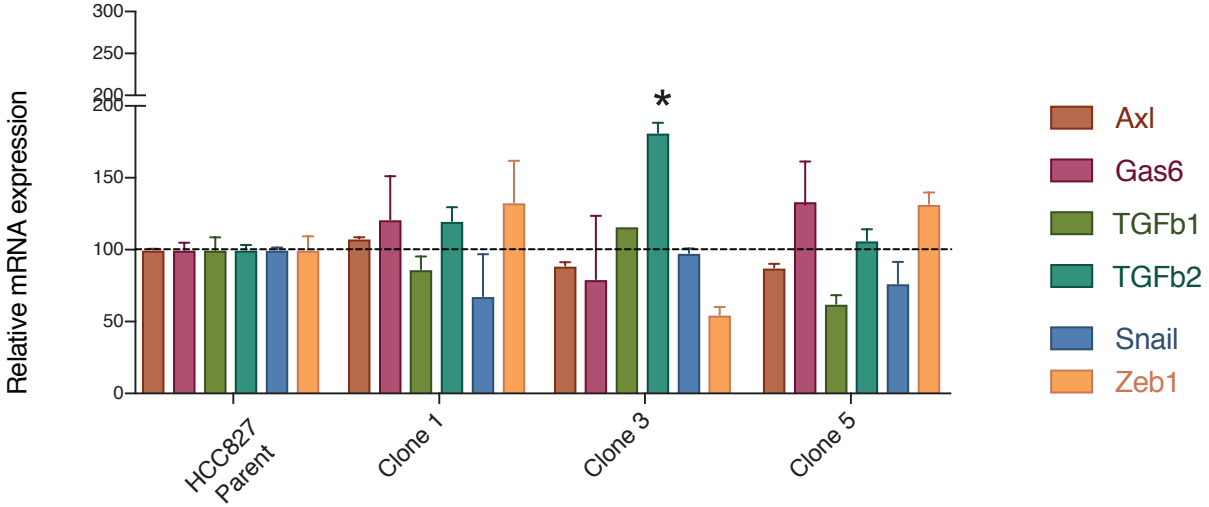

Figure 3-figure supplement 1

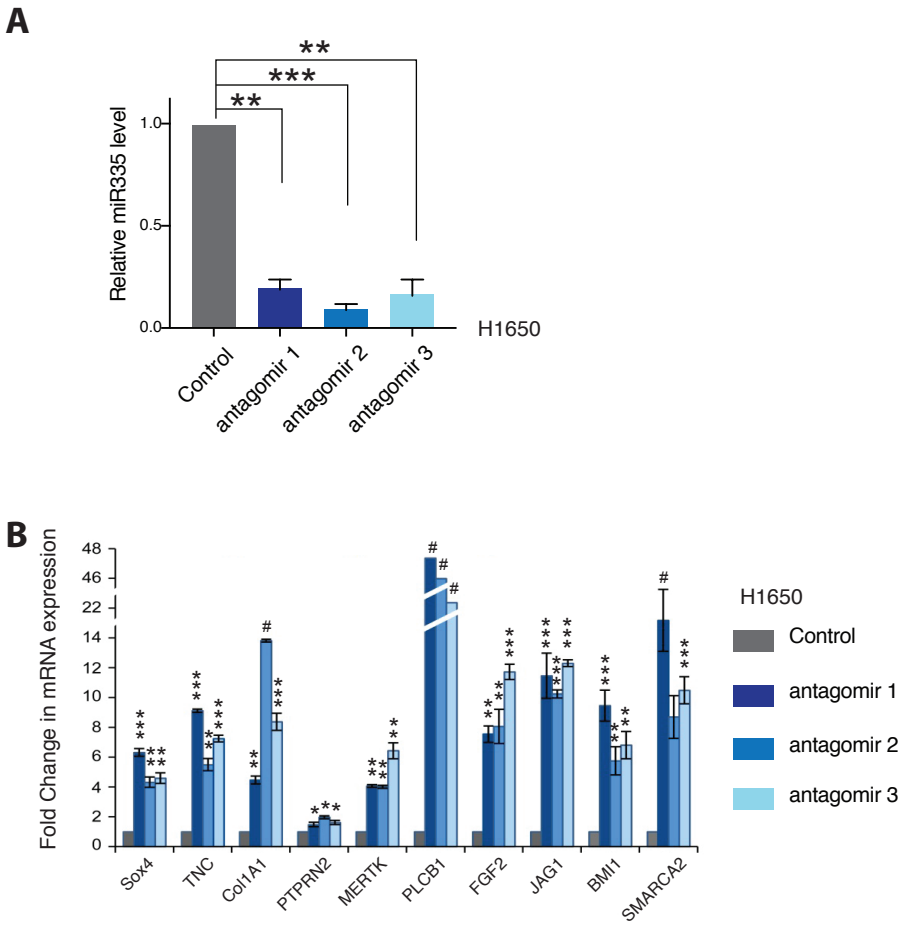

Figure 4-figure supplement 1

A **FACS profile for 1650 and pc9 + LNA**

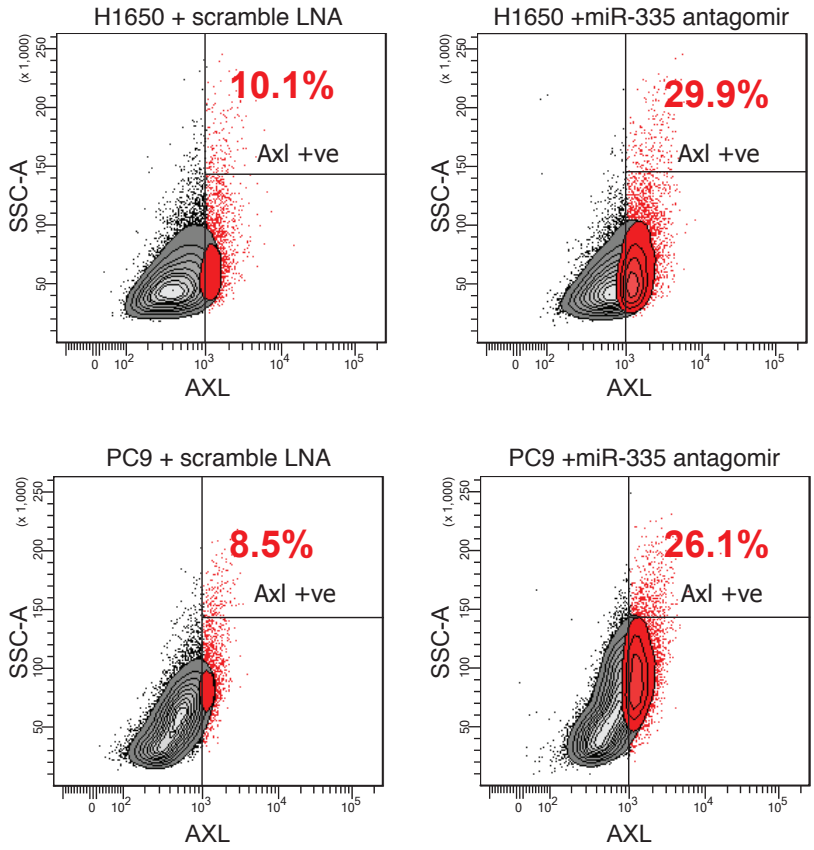

Figure 5-figure supplement 1

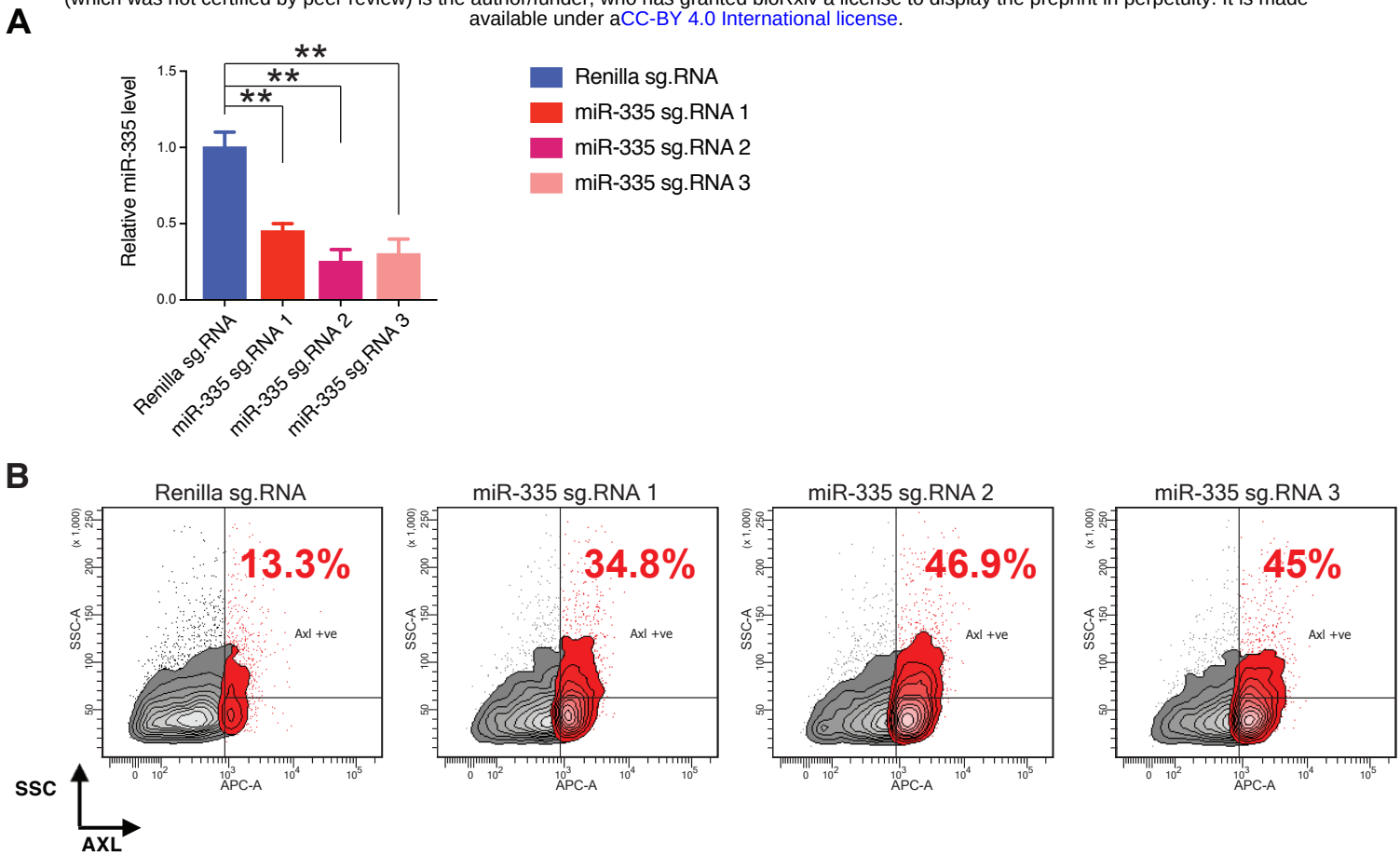

Figure 5-figure supplement 2

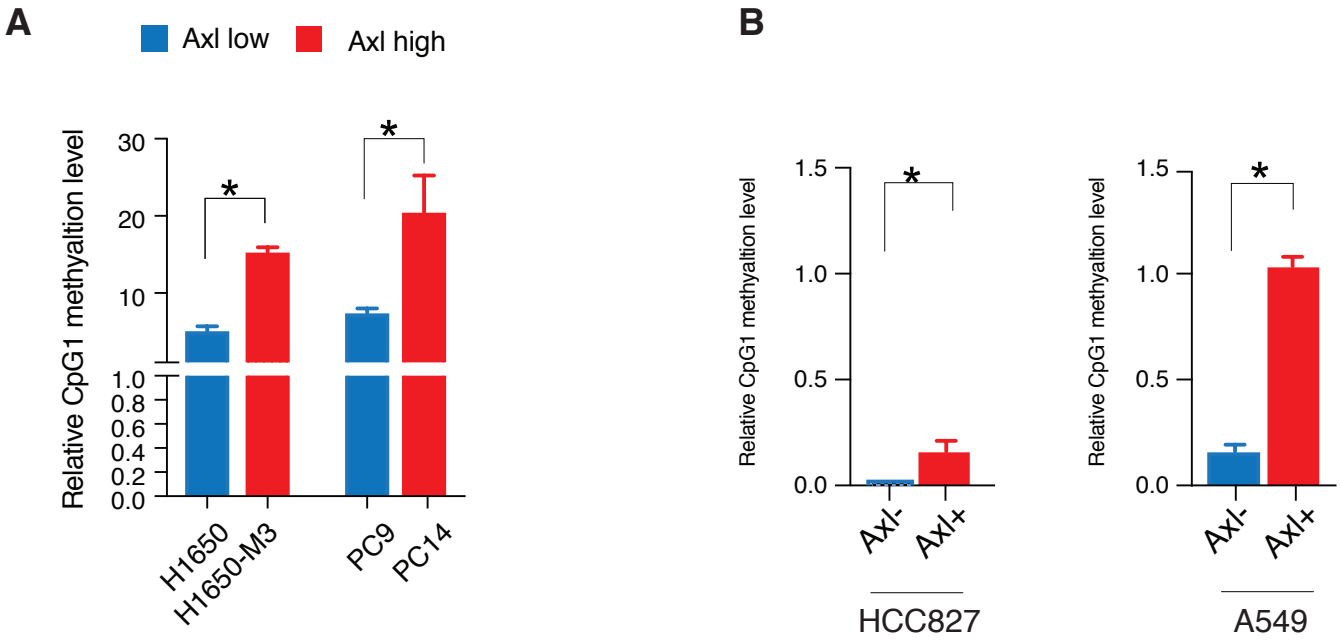

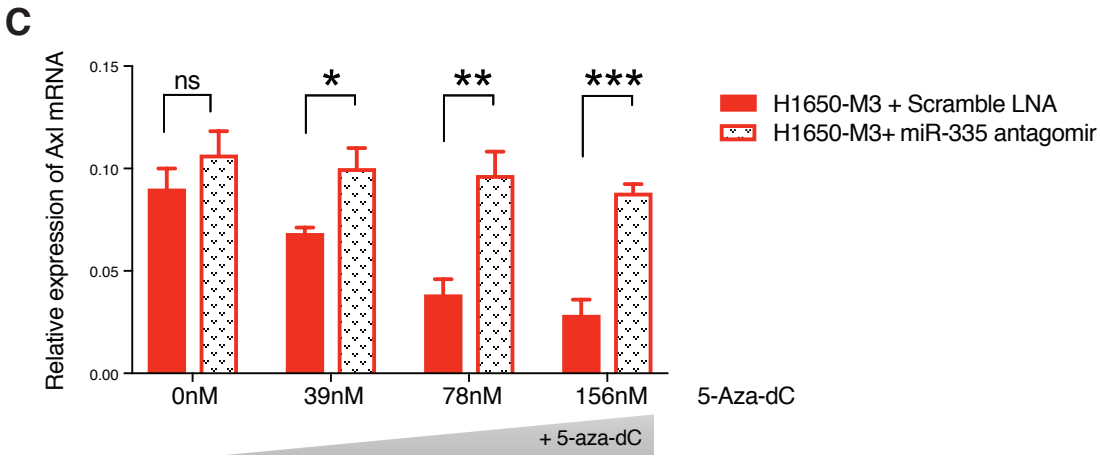

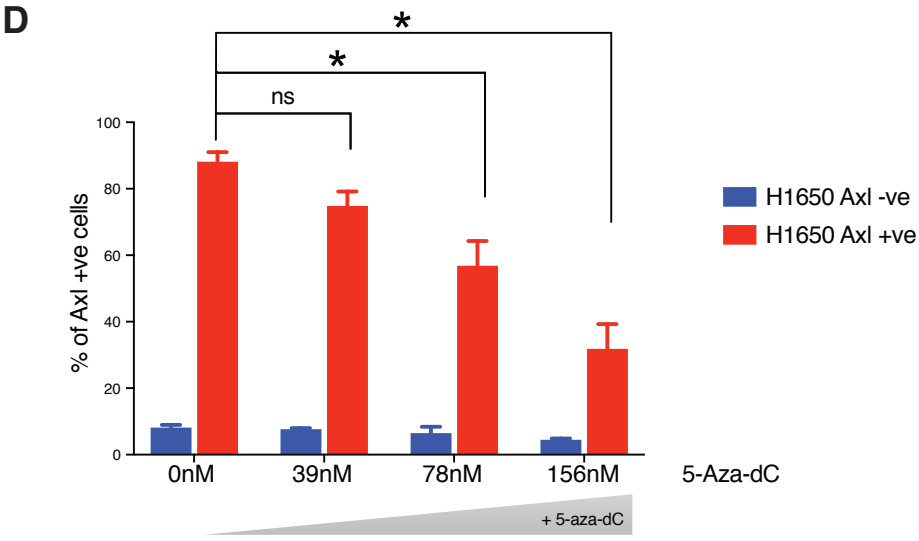

Figure 6-figure supplement 1